Interplay between intrinsic reprogramming potential and microenvironment controls neuroblastoma cell plasticity and identity

Authors: Cécile Thirant[1,2§], Agathe Peltier[1,2§], Simon Durand[1,2#], Amira Kramdi[1,2#], Caroline Louis-Brennetot[1,2#], Cécile Pierre-Eugène[1,2#], Ana Costa[1,2], Amandine Grelier[1,2], Sakina Zaïdi[1,2], Nadège Gruel[1,4], Irène Jimenez[2,3,4], Eve Lapouble[5], Gaëlle Pierron[5], Hervé J. Brisse[6], Arnaud Gauthier[7], Paul Fréneaux[7], Sandrine Grossetête-Lalami[1,2], Laura G. Baudrin[8], Virginie Raynal[1,8], Sylvain Baulande[8], Angela Bellini[2,3,4], Jaydutt Bhalshankar[2,3,4], Angel M. Carcaboso[9], Birgit Geoerger[10], Hermann Rohrer[11], Didier Surdez[1,2], Valentina Boeva[12,13,14], Gudrun Schleiermacher[2,3,4], Olivier Delattre[1,2], Isabelle Janoueix-Lerosey[1,2*]

Affiliations :

[1]Institut Curie, PSL Research University, Inserm U830, Equipe Labellisée Ligue contre le Cancer, Paris, France.
[2]SIREDO: Care, Innovation and Research for Children, Adolescents and Young Adults with Cancer, Institut Curie, Paris, France.
[3]Institut Curie, Laboratory Recherche Translationnelle en Oncologie Pédiatrique (RTOP), Laboratoire "Gilles Thomas", Paris, France.
[4]Institut Curie Department of Translational Research, Paris, France.
[5]Institut Curie, Unité de Génétique Somatique, Paris, France.
[6]Institut Curie, Department of Imaging, PSL Research University, Paris, France.
[7]Institut Curie, Department of Biopathology, Paris, France.
[8]Institut Curie, Genomics of Excellence (ICGex) Platform, Paris, France.
[9]Institut de Recerca Sant Joan de Déu, Barcelona, Spain.
[10]Gustave Roussy Cancer Campus, INSERM U1015, Department of Pediatric and Adolescent Oncology, Univ. Paris-Sud, Université Paris-Saclay, Villejuif, France.
[11]Institute of Clinical Neuroanatomy, Dr. Senckenberg Anatomy, Neuroscience Center, Goethe University, Frankfurt/M, Germany
[12]Inserm, U1016, Cochin Institute, CNRS UMR8104, Paris Descartes University, Paris, France.
[13]ETH Zürich, Department of Computer Science, Institute for Machine Learning, Zürich, Switzerland.
[14]Swiss Institute of Bioinformatics (SIB), Zürich, Switzerland.

[§,#] These authors contributed equally to this work.
***** Corresponding author and lead contact: janoueix@curie.fr

Abstract

Two cell identities, noradrenergic and mesenchymal, have been characterized in neuroblastoma cell lines according to their epigenetic landscapes relying on specific circuitries of transcription factors. Yet, their relationship and relative contribution in patient tumors remain poorly defined. Here, we demonstrate that the knock-out of *GATA3*, but not of *PHOX2A* or *PHOX2B*, in noradrenergic cells induces a mesenchymal phenotype. Our results document spontaneous plasticity in several models between both identities and show that plasticity relies on epigenetic reprogramming. We demonstrate that an *in vivo* microenvironment provides a powerful pressure towards a noradrenergic identity for these models. Consistently, tumor cells with a mesenchymal identity are not detected in a series of PDX models. Further study of the intra-tumor noradrenergic heterogeneity reveals two distinct cell populations exhibiting features of chromaffin-like or sympathoblast-like cells. This work emphasizes that both external cues of the environment and intrinsic factors control plasticity and cell identity in neuroblastoma.

INTRODUCTION

Neuroblastoma is a childhood cancer arising from the peripheral sympathetic nervous system, known to be derived from multipotent neural crest cells (NCCs). Tumors mostly develop in the adrenal gland but a subset of them originates from sympathetic ganglia along the paravertebral sympathetic chain[1]. With respect to these localizations, neuroblastoma likely arises from the transformation of sympathoblasts either in sympathetic ganglia or in the adrenal medulla, or from catecholamine-secreting chromaffin cells of the adrenal medulla, or alternatively from a common sympatho-adrenal progenitor[2,3].

The hallmark of neuroblastoma is its wide range of clinical presentations and outcomes, ranging from spontaneous regression to fatal outcome despite multimodal therapies[1]. High-risk neuroblastoma most often initially responds to intensive chemotherapy; however, relapses frequently occur followed by fatal outcome. Several genes including *MYCN*[4], *ALK*[5–8] and *TERT*[9–11] have been identified as key drivers of neuroblastoma oncogenesis.

The master transcriptional regulators controlling the gene expression program of neuroblastoma have been recently highlighted through the characterization of the neuroblastoma super-enhancer landscape of neuroblastoma cell lines, revealing two distinct cell identities: a sympathetic noradrenergic identity defined by a core regulatory circuitry (CRC) module including the

PHOX2B, HAND2 and GATA3 transcription factors (TFs) and a NCC-like/mesenchymal identity, close to that of human neural crest cells (NCCs), driven by TFs of the AP1 family among others[12,13]. Additional TFs participating in the noradrenergic CRC have been then identified, including ISL1, TBX2 and ASCL1[14–16]. It is likely that PHOX2A, also highly expressed in neuroblastoma cell lines and exhibiting the same DNA binding domain as PHOX2B is involved in the noradrenergic CRC. Importantly, mesenchymal tumor cells *in vitro* have been shown to be more resistant to standard chemotherapy[12,13] suggesting that they may be involved in therapeutic resistance and relapses in neuroblastoma patients. Bulk RNA-seq analyses or immunohistochemistry with few markers suggested that mesenchymal tumor cells are present in patient tumors and that some tumors exhibit a mesenchymal identity[12,13,17]. Cellular plasticity between the noradrenergic and mesenchymal states has been reported for a few cell lines[13,18], still the underlying mechanisms wherein the cell phenotype switches from one to the other state (considered as transdifferentiation) remain poorly described. In the present paper, we have combined various approaches including genetic inactivation of specific TFs and single-cell transcriptomic analyses to unravel TFs involved in cell identity and plasticity and better decipher the relationship and relative contribution of cells of noradrenergic and mesenchymal identity in neuroblastoma tumors.

RESULTS

The knock-out of *GATA3* but not of *PHOX2B* or *PHOX2A* induces a switch from a noradrenergic to a mesenchymal identity

In order to directly address the functional role of the PHOX2A, PHOX2B and GATA3 TFs in shaping the noradrenergic identity, we performed their individual genetic knock-out (KO) in the noradrenergic SH-SY5Y cell line using a CRISPR-Cas9 approach. Guide RNAs were designed to induce large deletions and create frameshift mutations in those genes, leading to truncated and nonfunctional proteins. We obtained two *PHOX2A*$^{-/-}$ clones, a *PHOX2B*$^{-/-}$ clone and two *GATA3*$^{-/-}$ clones (**Figure S1A**). While the *PHOX2A*$^{-/-}$ and *PHOX2B*$^{-/-}$ clones showed a morphology close to that of the parental noradrenergic SH-SY5Y cells with neurite-like processes, *GATA3*$^{-/-}$ cells exhibited a more abundant cytoplasm and many actin stress fibers consistent with a mesenchymal phenotype (**Figure 1A**). *PHOX2A*$^{-/-}$ and *PHOX2B*$^{-/-}$ clones maintained the expression of the noradrenergic CRC TFs including GATA3 and HAND2 (**Figures 1B and S1B**). Strikingly, both *GATA3*$^{-/-}$ clones showed an absence or highly reduced expression of the TFs from the noradrenergic CRC, including PHOX2A, PHOX2B, and HAND2 (**Figure 1B**). *PHOX2B*$^{-/-}$ and *GATA3*$^{-/-}$ cells were characterized by a decreased proliferation compared to the parental SH-SY5Y cell line (**Figure 1C**). Consistently with their phenotype, *GATA3*$^{-/-}$ clones displayed

mesenchymal properties such as an increased invasion ability measured in a 3D-spheroid assay (**Figure 1D**), increased migration capacity documented using a transwell assay (**Figure 1E**) and a higher resistance to chemotherapy *in vitro* (**Figure 1F**). Bulk RNA-seq analysis showed that *PHOX2A*$^{-/-}$ and *PHOX2B*$^{-/-}$ clones harbored transcriptomic profiles highly similar to that of the parental noradrenergic SH-SY5Y cell line, confirming that *PHOX2A* or *PHOX2B* genetic invalidation did not change the cell identity. In contrast, *GATA3*$^{-/-}$ clones, at two different passages called early and late showed a mesenchymal transcriptomic profile, as they clustered with the mesenchymal SH-EP cell line (**Figures 1G and S1C**). Accordingly, Gene Ontology analysis on the 2,938 differentially expressed genes between the transcriptomic profiles of the 4 *GATA3*$^{-/-}$ samples versus 5 noradrenergic neuroblastoma cell lines (without *MYCN* amplification as the parental SH-SY5Y) retrieved categories related to neuron differentiation, neurogenesis, sympathetic nervous development for the downregulated genes and extracellular matrix organization, cell motility and cell migration for the upregulated genes (**Figure S1D**).

These observations therefore demonstrated that the KO of the *PHOX2A, PHOX2B* or *GATA3* transcription factors has different consequences on the maintenance of the noradrenergic identity and that SH-SY5Y cells are able to transdifferentiate from a noradrenergic to a mesenchymal state upon *GATA3* KO.

Spontaneous plasticity between the noradrenergic and mesenchymal states reveals the reprogramming potential of a subset of neuroblastoma cells

Our previous study has shown that most of the neuroblastoma cell lines (18 out of 25) exhibit a noradrenergic identity whereas only 3 have a mesenchymal epigenetic profile. An intermediate group of cells expressing noradrenergic TFs and mesenchymal TFs was composed of 4 samples, including the heterogeneous SK-N-SH cell line[12]. Interestingly, plasticity properties have been reported for this cell line[18]. Using single-cell transcriptomic sequencing with the 10X Genomics technology, we highlight here two cell populations in the SK-N-SH cell line. Noradrenergic cells expressed *PHOX2B* whereas *CD44*[19–21] appeared as a specific marker of the mesenchymal population confirmed by FACS and immunofluorescence (**Figure 2A-C**). An InferCNV analysis that predict the genetic alterations at the single-cell level[22], showed that both populations exhibited similar genetic alterations (2p, 7 and 17q gains). Only one subcluster of the mesenchymal population presented with a 1q gain (**Figure 2D**), consistently with previous data reporting distinct genetic subclones[23]. As CD44 is a cell surface marker it was further used to sort both populations. Bulk RNA-seq experiments confirmed that CD44^{neg} and CD44^{pos} sorted cells exhibited transcriptomic profiles close to noradrenergic SH-SY5Y and

mesenchymal SH-EP cells, respectively (**Figure 2E**). Both sorted noradrenergic/CD44^{neg} and mesenchymal/CD44^{pos} populations were able to give rise to a heterogeneous cell population, demonstrating a spontaneous and bidirectional plasticity between the noradrenergic and mesenchymal states (**Figure 2F**). As expected from previous data obtained with the SH-SY5Y and SH-EP cell lines sub-cloned from the heterogeneous parental SK-N-SH cell line[12], the mesenchymal/CD44^{pos} population of this cell line exhibited a higher chemo-resistance compared to the noradrenergic/CD44^{neg} one (**Figure 2G**).

In order to demonstrate that plasticity between the noradrenergic and mesenchymal states is not a property exclusively observed in the SK-N-SH sample, we generated new cell lines from a series of 10 neuroblastoma PDX models. Cells from two models could be maintained in culture for several months and frozen. One cell line had a pure noradrenergic phenotype. Strikingly, the other cell line called IC-pPDXC-63 was able to grow *in vitro* as a bi-phenotypic culture, with both adherent cells and floating neurospheres (**Figure 3A**)**.** Bulk RNA-seq analysis confirmed that the original PDX model (IC-pPDX-63) and its derived-cell line exhibited a transcriptomic profile highly similar to the one of the patient tumor (NB1549) (**Figure 3B**)**.** As shown by single-cell analysis, two main clusters of noradrenergic cells and mesenchymal tumor cells were observed in the IC-pPDXC-63 cell line, with a bridge of cells in-between (**Figure 3C**). Noradrenergic cells expressed *PHOX2B*, whereas the mesenchymal population expressed the cell surface CD44 marker (**Figure 3C**). The clustering separating noradrenergic and mesenchymal tumor cells is not biased by the cell cycle (**Figure 3C**). Immunofluorescence confirmed that CD44 and PHOX2B were specifically expressed by adherent cells and neurospheres, respectively (**Figure 3D**). Bulk RNA-seq analysis endorsed that CD44^{pos} FACS-sorted cells and adherent cells have a transcriptomic profile close to the mesenchymal SH-EP cells, whereas CD44^{neg} FACS-sorted cells and floating neurospheres clustered with the noradrenergic SH-SY5Y cells (**Figure 3B**). Consistently with the observations in the SK-N-SH cell line, we documented that the mesenchymal population of the IC-pPDXC-63 cell line exhibited a higher chemo-resistance compared to the noradrenergic one (**Figure 3E**). Of note, inferred genomic alterations were similar in the three populations of the IC-pPDXC-63 cell line, *i.e.*, the noradrenergic, mesenchymal and bridge cells (**Figure 3F**). We next investigated the plasticity properties of both noradrenergic and mesenchymal cells of the IC-pPDXC-63 cell line *in vitro*. After a few days in culture, both sorted noradrenergic/CD44^{neg} and mesenchymal/CD44^{pos} cells were able to reconstitute a heterogeneous cell population (**Figure 3G**), as previously documented for the SK-N-SH cell line. These observations therefore highlight the reprogramming potential between the noradrenergic and mesenchymal states of the IC-pPDXC-63 model and importantly, show that this ability does not rely on genetic heterogeneity.

168 **Phenotypic plasticity relies on epigenetic reprogramming**

169 To deeper characterize the epigenetic reprogramming contribution to cell plasticity, we next
170 defined the super-enhancer landscape of our three different models (*GATA3* genetic inactivation, SK-
171 N-SH and IC-pPDXC-63 cell lines) by ChIP-seq analyses for the H3K27ac mark. We added these samples
172 in the principal component analysis (PCA) of neuroblastoma cell lines and hNCC lines based on their
173 super-enhancer log scores[12] (**Figure 4A**). For all three models, their mesenchymal counterparts, *i.e.*
174 *GATA3*$^{-/-}$ clones, SK-N-SH CD44^{pos} FACS-sorted and adherent IC-pPDXC-63 cells, showed an epigenetic
175 profile close to the group II of mesenchymal identity. Consistently, their noradrenergic counterparts,
176 SH-SY5Y, SK-N-SH CD44^{neg} FACS-sorted and floating IC-pPDXC-63 cells were part of the noradrenergic
177 cell line group I (**Figure 4A**). For the mesenchymal cells of the three models, a decrease of the H3K27ac
178 signal could be quantified for the super-enhancer regions of the noradrenergic CRC such as *GATA3*,
179 *PHOX2B* and *HAND1*. On the other hand, an increase of the H3K27ac signal could be observed on some
180 NCC-like/mesenchymal TFs such as *RUNX1*, *FOSL1*, *NR3C1,* and *TBX18* (**Figure 4B,C**). Of note, the
181 decreased PHOX2A and HAND2 protein expressions in the *GATA3*$^{-/-}$ clones (**Figure 1B**) contrasted with
182 high transcript levels (**Figure 1G**) and high H3K27ac scores (**Figure 4B**) suggesting a distinct
183 transcriptional and post-transcriptional regulation for these specific genes.

184 Altogether, these results indicate that the transdifferentiation from a noradrenergic to a
185 mesenchymal identity obtained after the genetic inactivation of *GATA3* or spontaneously from SK-N-
186 SH and IC-pPDXC-63 cells is supported by an epigenetic reprogramming.

187

188 **Mesenchymal neuroblastoma cells are reprogrammed to a noradrenergic phenotype *in vivo***

189 Since noradrenergic and mesenchymal cells of our three models presented with different
190 properties *in vitro*, we next investigated their behavior *in vivo*. We injected the noradrenergic/CD44^{neg}
191 and mesenchymal/CD44^{pos} sorted cell populations from the two heterogeneous SK-N-SH and IC-
192 pPDXC-63 cell lines, as well as the *GATA3*$^{-/-}$ cells, into mice. Tumors developed in all cases, indicating
193 that the different states displayed tumorigenic potential *in vivo*. Unexpectedly, as revealed by IHC
194 analysis, PHOX2B expression was observed in most tumor cells from the whole set of xenografts, even
195 those obtained after engraftment of mesenchymal populations (**Figure 5A**). Bulk RNA-seq experiments
196 confirmed that all tumors highly expressed the TFs of the noradrenergic CRC and exhibited a
197 noradrenergic transcriptomic profile (**Figures 5B and S2**). Xenografts of the *GATA3*$^{-/-}$ clones re-
198 expressed the noradrenergic and neuroendocrine *DBH, NET/SLC6A2, CHGA* and *CHGB* markers
199 compared to the clones cultured *in vitro* (**Table S1**). Consistently, PHOX2B and DBH proteins were
200 detected in the *GATA3*$^{-/-}$ cell xenografts (**Figure 5C**). Additionally, these markers were similarly

201 expressed in xenografts obtained with the two CD44^{pos} and CD44^{neg} cell populations of the SK-N-SH
202 and IC-pPDXC-63 cell lines (**Table S1**). Differential analyses (Fold-change >2; Bonferroni-corrected p-
203 value <0.05) showed that xenografts obtained from CD44^{pos} and CD44^{neg} cells of both heterogeneous
204 cell lines were highly similar, with less than 50 genes (data not shown) showing a differential
205 expression, compared to more than 2,000 genes differentially expressed *in vitro*. Of note, some genes
206 of the neurogenesis and extracellular matrix organization were still differentially expressed between
207 SH-SY5Y and *GATA3*$^{-/-}$ cell xenografts, but of lower magnitude compared to the difference between the
208 corresponding cells *in vitro*. Finally, to fully demonstrate the *in vivo* reprogramming of mesenchymal
209 cells towards a noradrenergic identity, we determined the super-enhancer profiles of SH-SY5Y and
210 *GATA3*$^{-/-}$ cell xenografts and additionally from the xenografts of SK-N-SH CD44^{pos} and CD44^{neg} FACS-
211 sorted cells. The PCA clearly showed that all these tumors were part of the noradrenergic group I
212 (**Figure 5D**). Super-enhancers marked *PHOX2B* and *HAND1* genes in xenografts of SH-SY5Y and SK-N-
213 SH CD44^{neg} cells but also in xenografts of *GATA3*$^{-/-}$ and SK-N-SH CD44^{pos} cells (**Figure 5E**). In an *in vivo*
214 environment, the mesenchymal cells therefore shifted back towards a noradrenergic identity
215 indicating that the mouse microenvironment provided strong cues inducing a global epigenetic
216 reprogramming.

217 Altogether, our analyses highlighted the plasticity properties of neuroblastoma cells using
218 three different models (*GATA3* genetic inactivation, SK-N-SH and IC-pPDXC-63 cell lines). This plasticity
219 was associated with a reprogramming potential from a mesenchymal state to a noradrenergic state
220 following *in vivo* engraftment in the mouse.

221

222 **Single-cell transcriptomic analyses reveal intra-tumor noradrenergic heterogeneity but no**
223 **mesenchymal tumor cells in neuroblastoma PDX models**

224 Since heterogeneity of cell identity has been observed in some neuroblastoma cell lines, we
225 took advantage of the 10X Genomics technology to explore neuroblastoma intra-tumor heterogeneity
226 using single-cell transcriptomic analyses on 14 PDX models, obtained at diagnosis, progression or at
227 relapse (**Figure 6A, Table S2**). The study was designed to specifically identify human tumor cells (see
228 methods). The integration of the human cells from all models (n=47,219 cells) with the Harmony tool[24]
229 highlighted tumor cells of noradrenergic identity (*PHOX2B+*, *HAND2+*) (**Figures 6B-C** and **S3A**). No
230 cluster of mesenchymal tumor cells could be identified as shown by the analysis of previously
231 published mesenchymal signatures (**Figure 6D**). The InferCNV analyses confirmed that noradrenergic
232 tumor cells exhibited the emblematic genetic alterations of neuroblastoma such as 17q gain[1] (**Figure**
233 **S3B-C**). For several models, we could compare the InferCNV profile calculated from scRNAseq data to

copy number profiles inferred from whole-exome sequencing data and confirmed their full consistency (**Figure S3B**). We next assessed the heterogeneity of the human tumor cell populations and documented that most clusters were shared by all PDX models (**Table S4**). Several populations could be defined according to the differential expression of specific genes: cycling cells marked by the expression of *TOP2A, MKI67* and *CDK1* (clusters 2 and 6), cells driven by a *MYCN/*2p amplicon signature (clusters 0-1-2-3-13), cells expressing chromaffin markers such as *CDKN1C*, *SLC18A1*/VMAT1[25,26] and *DLK1*[27] (clusters 9-10-11) and cells with a sympathoblast-like identity such as *TFAP2B*[28] (cluster 7) (**Figures 6E, S3D-F** and **Table S4**).

Interestingly, our single-cell transcriptomic data revealed that the GR-NB7 PDX model did not express *GATA3* but expressed *PHOX2B*, *CHGA* and *DDC* (**Figure 6F).** These data confirmed that *GATA3* was dispensable to establish a noradrenergic identity *in vivo*, in agreement with the noradrenergic shift of *GATA3*$^{-/-}$ cells observed in mouse xenografts. Unsupervised hierarchical clustering using the 10% genes with the highest IQR on bulk RNA-seq data confirmed that all studied PDX models exhibited a transcriptomic profile corresponding to a noradrenergic identity (**Figure S3F**).

Altogether, the present analysis of 24 neuroblastoma samples identified no *bona fide* tumor mesenchymal cells, which is consistent with our aforementioned results demonstrating a strong pressure of the microenvironment towards a noradrenergic identity.

DISCUSSION

In the present work, we have first deciphered the distinct roles of the members of the noradrenergic CRC in shaping neuroblastoma cell identity. Whereas *Phox2b* is essential for initial sympatho-adrenal cell specification from neural crest progenitors[29–31], the KO of *PHOX2B* or *PHOX2A* did not modify the noradrenergic identity of SH-SY5Y cells. Yet, one hypothesis is functional redundancy between PHOX2A and PHOX2B. Of note, we did not succeed in obtaining double KO clones suggesting synthetic lethality for the cells. In contrast, the KO of *GATA3* in the same cells had a dramatic effect, inducing the collapse of the noradrenergic CRC. Surprisingly, whereas *GATA3* KO clones harbored mesenchymal properties *in vitro*, they reacquired a noradrenergic identity *in vivo* indicating that *GATA3* KO allows a permissive epigenetic state and the transdifferentiation towards a mesenchymal or noradrenergic state according to non-autonomous cues. Consistently with these observations, we could document a noradrenergic identity of one neuroblastoma PDX model characterized by an absence of GATA3 expression. In a previous study using siRNA and short-term transcriptomic analysis by RT-q-PCR, Durbin *et al*. reported that the knock-down of only one member of the CRC was able to induce a decrease of the expression of several members of the CRC[15]. Yet,

residual expression remained for the different TFs studied and the impact of this decrease on cell identity has not been explored. Therefore, our results constitute the first evidence that TFs of a specific CRC may have distinct roles in shaping cell identity in neuroblastoma.

Transdifferentiation from the noradrenergic to the mesenchymal identity has been shown previously *in vitro* following overexpression of the PRRX1 TF[13]. The same team also recently pointed out a role of the NOTCH signaling pathway in this process[32]. Of note, xenografts of SH-SY5Y cells overexpressing NOTCH3 intracellular domain exhibited a mesenchymal identity. In this model, the permanent production of intra-cellular NOTCH3 likely activates an endogenous feed-forward loop between NOTCH receptors and ligands *in vivo.* Although we observed expression of several members of this pathway (*NOTCH2*, *MAML2*, *HES1*) in our mesenchymal tumor cells *in vitro*, in our series of PDX models, only expression of *MAML2* could be detected in some tumor cells; yet these cells were not associated with a specific cluster and very spare expression was observed for *NOTCH2* and *HES1* in the whole population of tumor cells.

We document here the heterogeneity and spontaneous reprogramming potential of cells of IC-PDXC-63 and SK-N-SH models from a noradrenergic to a mesenchymal identity and conversely. Single-cell transcriptomic analysis performed on these models first identified CD44 as a surface marker specific of the mesenchymal identity, further allowing the use of this marker to sort each population and analyze their respective proportions by FACS. We show that the spontaneous and bi-directional plasticity observed *in vitro* relies on a profound epigenetic reprogramming, as revealed by the analysis of the super-enhancer landscape of the various cell populations. Very strikingly, we demonstrate that mesenchymal tumor cells from three different models exhibiting plasticity revert their identity towards a noradrenergic state when engrafted in mice. These results highlight that neuroblastoma cell phenotype is strongly influenced by the *in vivo* microenvironment which provides a powerful pressure towards a noradrenergic state. This conclusion is reinforced by the observation that mesenchymal tumor cells were not identified by single-cell transcriptomic analyses in our series of 14 neuroblastoma PDX models, obtained either at diagnosis or at relapse and presenting various genetic alterations. Altogether, our data obtained on a variety of cellular models and PDXs provide a biological explanation for the absence of mesenchymal tumor cells *in vivo*. This observation is also in line with the very recent study performed by Dong and colleagues that identified normal, but not tumor, mesenchymal cells in adrenal neuroblastoma tumors by single-cell RNA sequencing[33]. Interactions between tumor cells and several cell populations of the microenvironment may influence the tumor cell phenotype and play a role in tumor progression, as previously demonstrated for tumor-associated inflammatory cells[34]. Future studies should decipher the cues of the microenvironment and their associated pathways that converge to regulate cell plasticity during tumor progression.

Interestingly, some evidences suggested that treatments against neuroblastoma may impact cell identity. Indeed, previous analyses of neuroblastoma cells selected to be resistant to cisplatin[35] or ALK inhibitors[36] *in vitro* have reported that noradrenergic cells may acquire mesenchymal properties. Cells exhibiting such a potential may be transiently induced upon chemotherapy treatment and revert their state towards a noradrenergic identity when the treatment pressure decreases, the mesenchymal cells being the drug-resistant reservoirs for noradrenergic cells. Further experiments will allow better defining their contribution to therapeutic resistance and relapse in high-risk neuroblastomas.

The cell of origin in neuroblastoma has been for long a matter of debate[37–39]. Some models argue that this tumor arises from the transformation of NCCs while other models suggest that they develop from more engaged sympatho-adrenal progenitors, able to generate both sympathetic neurons and neuroendocrine cells of the adrenal. Recently, this hierarchical dogma of normal differentiation has been questioned with the identification of a population of Schwann cell precursors (SCPs) as the main reservoir of adrenal chromaffin cells in the mouse[26]. In their recent paper, Dong et al. who analyzed human fetal adrenal gland at the single-cell level, in addition to adrenal neuroblastoma tumors, concluded that malignant cells had a predominant chromaffin-cell-like phenotype[33]. We nevertheless disagree with their interpretation of cell phenotypes. We strongly believe that *CARTPT* and *INSM1,* used by Dong et al. to define sympathoblast identity, rather witness a chromaffin-like phenotype, since they are co-expressed with *DLK1*, *CDKN1C*, *CHGA*/*CHGB*, *TH*, *DBH* and *SLC18A1* in our data [25–27,40–44]. Integration of our single-cell RNA-seq data from 14 PDX models revealed two distinct cell populations expressing either markers of chromaffin cells or markers of sympathoblasts. Of note, SCP markers such as *SOX10, S100B, PLP1* and *ERBB3*[26] were not detected in our cohort of 14 neuroblastoma cases. Nevertheless, it remains difficult to infer which cell type is the one targeted by neoplastic transformation. Indeed, it cannot be excluded that transitions may occur between chromaffin cells and sympathoblasts during development and/or that markers of a specific precursor may be lost during cell transformation.

Altogether, our data obtained on several cellular models demonstrate that a subset of neuroblastoma cells exhibits a reprogramming potential between a noradrenergic and a mesenchymal identity and that both intrinsic properties and exogenous signals of the microenvironment dictate this identity. A better understanding of the molecular factors that control phenotypic plasticity will represent a key step in the design of more efficacious therapies that aim at improving the outcome of neuroblastoma patients with high-risk disease.

ACKNOWLEDGEMENTS

This work was supported by grants from Institut Curie, Inserm, the Ligue Nationale Contre le Cancer (Equipe labellisée), the Institut National du Cancer (PLBIO18-273) and by the following associations: Association Hubert Gouin-Enfance et Cancer, Les Bagouz à Manon, les amis de Claire, Courir pour Mathieu, Dans les pas du Géant, Olivier Chape. The Mappyacts protocol is supported by the Institut National de Cancer (INCa) through the PHRC "INCa-DGOS_8519" MERRI, the Fondation ARC, the Association Imagine for Margo, the Société Française de lutte contre les Cancers et les leucémies de l'Enfant et l'adolescent (SFCE), Fédération Enfants & Santé, the associations AREMIG and Thibault BRIET. The Micchado protocol is supported by PRT-K, Association Imagine for Margo, Kickcancer, Hubert Gouin-Enfance et Cancer, Fédération Enfants & Santé, and funding support by BMS and Roche. High-throughput sequencing has been performed by the ICGex NGS platform of the Institut Curie supported by the grants ANR-10-EQPX-03 (Equipex) and ANR-10-INBS-09-08 (France Génomique Consortium) from the Agence Nationale de la Recherche ("Investissements d'Avenir" program), by ITMO Cancer Aviesan ("Equipement pour la recherche en Cancérologie" program) and by the SiRIC-Curie program -SiRIC Grant "INCa-DGOS- 4654". G.S. is supported by the Annenberg foundation. H.R. is supported by the Wilhelm-Sander-Stiftung. We are grateful to the animal facilities team, the Experimental Pathology Department, the Plateforme Génomique and the Plateforme Cytométrie of Institut Curie, U900 colleagues for help with alignment of NGS data and Julien Masliah-Planchon for help with genomic analyses. We thank Mélissa Saichi and Divya Sahu for preliminary analyses of single-cell RNA-seq and ChIP-seq data.

AUTHOR CONTRIBUTIONS

Conceptualization: C.T., V.B., O.D. and I.J.-L.; Methodology: C.T., A.P., S. Z., N.G., I. J., A.M.C., B.G. and D.S.; Formal Analysis: C.T., A.K., A.C., S.G.-L., V.B.; Investigation: C.T., A.P., S.D., C.L.-B., C.P.-E., A.C., A.G., N.G. and H.R.; Resources: E.L., G.P., H.B., A.G., P.F., L.G. B., V.R., S.B., A. B., J.B and G.S.; Writing – Original Draft: C.T., A.P. and I.J.-L.; Writing – Review and Editing: C.T., A.P., C.L.-B., H.R., O.D. and I.J.-L.; Visualization: C.T., A.P., A.K., C.L.-B., C.P.-E.; Supervision: C.T. and I.J.-L.; Project Administration: I.J.-L.; Funding Acquisition: I.J.-L, V. B. and O.D.

DECLARATION OF INTERESTS

The authors declare no potential conflicts of interest.

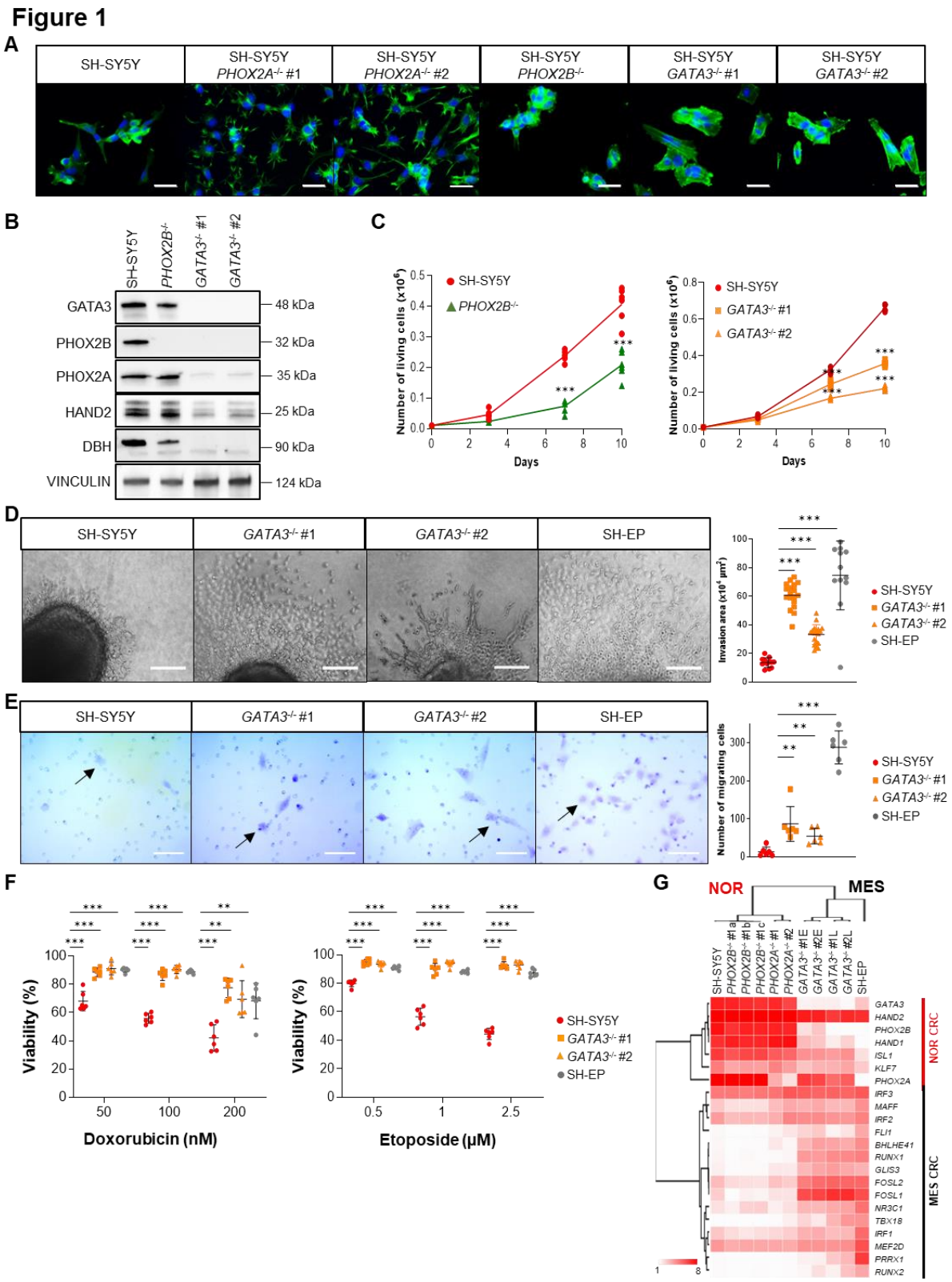

Figure 1. *GATA3*$^{-/-}$ cells exhibit mesenchymal properties whereas *PHOX2B*$^{-/-}$ or *PHOX2A*$^{-/-}$ cells keep a noradrenergic phenotype *in vitro*. (**A**) Phalloidin staining reveals the cell phenotype of the different KO clones and the SH-SY5Y parental cell line (x400, scale bar = 20 µm). (**B**) Western blot analysis of GATA3, PHOX2B, PHOX2A, HAND2 and DBH in the *PHOX2B*$^{-/-}$ and *GATA3*$^{-/-}$ clones, with Vinculin as a

loading control. (**C**) Proliferation curves for *PHOX2B*$^{-/-}$ and *GATA3* $^{-/-}$ cells *in vitro*. 10,000 cells were seeded in 24-well plates. Living cells were counted after 3, 7 and 10 days of culture (mean ± sd.; n = 6 replicates). (**D**) Representative images (left) and quantification (right) of spheroid invasion assays. Cells were seeded in low adherent plates to form neurospheres for 4 days and embedded in collagen I for 72h. Scale bar = 100 µm (mean ± sd.; n = 12 replicates for SH-SY5Y and SH-EP cell lines and n = 18 replicates for *GATA3*$^{-/-}$ clones #1 and #2). (**E**) Representative images (left) and quantification (right) of transwell assays for the SH-SY5Y cells, the *GATA3*$^{-/-}$ clones (#1 and #2) and mesenchymal control cells (SH-EP). 50,000 cells were plated in a transwell insert and the living cells that have migrated into the transwell membrane were counted 24h later. Scale bar = 20 µm (mean ± sd.; n = 6 replicates). Each dot represents a replicate and is the mean of 6 different images of the well. (**F**) *GATA3*$^{-/-}$ cells are more resistant to chemotherapy than the SH-SY5Y noradrenergic parental cell line. Cell viability was measured after 48 hours of chemotherapy treatments (Doxorubicin 50, 100, 200 nM and Etoposide 0.5, 1, 2.5 µM) (mean ± sd.; n = 6 replicates). (**G**) Heatmap showing the expression levels of the TFs of the noradrenergic (n=7) and mesenchymal (n=15) CRC in the *PHOX2B*$^{-/-}$ (clone#1, 3 replicates), *PHOX2A*$^{-/-}$ (clones #1 and #2) and *GATA3*$^{-/-}$ (clones #1 and #2). Both *GATA3*$^{-/-}$ clones were analyzed at two different time points (early (E) and late (L)). The noradrenergic SH-SY5Y and the isogenic mesenchymal SH-EP cell lines were also included in the analysis. P-values were determined via two-tailed unpaired Welch's t-test (**: $p<0.01$, ***: $p<0.001$).

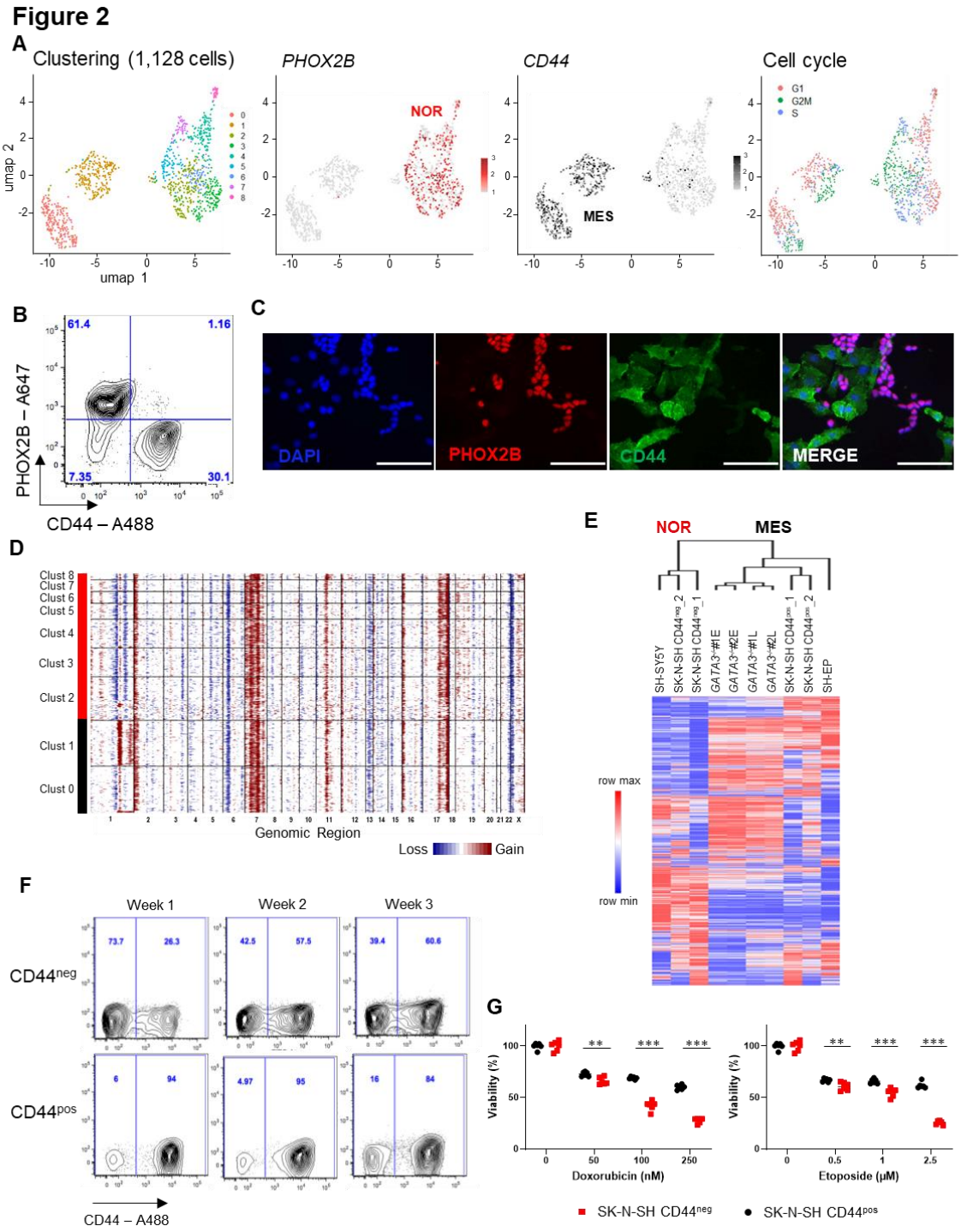

Figure 2. Cell plasticity in the heterogeneous neuroblastoma SK-N-SH cell line. (**A**) Single-cell RNA-seq analysis by Seurat. The umap plot shows two main clusters, *PHOX2B* and *CD44* expression distinguish noradrenergic and mesenchymal cells, each identity including cycling cells. (**B**), (**C**) FACS and immunofluorescence analyses of the SK-N-SH cell line with the PHOX2B and CD44 markers (scale bar= 50 µm). (**D**) Genetic alterations were predicted from single-cell RNAseq data using the InferCNV tool. (**E**) Unsupervised clustering using the top 10% of genes with the highest IQR (Inter-Quartile Range) indicates that CD44^{neg} and CD44^{pos} sorted cells (two replicates) exhibit a transcriptomic profile close to

the noradrenergic SH-SY5Y and mesenchymal SH-EP cells, respectively. (**F**) $CD44^{neg}$ (upper panel) and $CD44^{pos}$ (lower panel) sorted cells are able to reconstitute a heterogeneous population of both $CD44^{neg}$ and $CD44^{pos}$ cells after a few weeks in culture. (**G**) Mesenchymal/$CD44^{pos}$ sorted cells are more resistant to doxorubicin and etoposide than noradrenergic/$CD44^{neg}$ cells. Cell viability was measured after 72 hours of chemotherapy treatments (Doxorubicin 50, 100, 250 nM and Etoposide 0.5, 1, 2.5 µM)) (mean ± sd.; n = 6 replicates). P-values were determined via two-tailed unpaired Welch's t-test (**: $p<0.01$; ***: $p<0.001$).

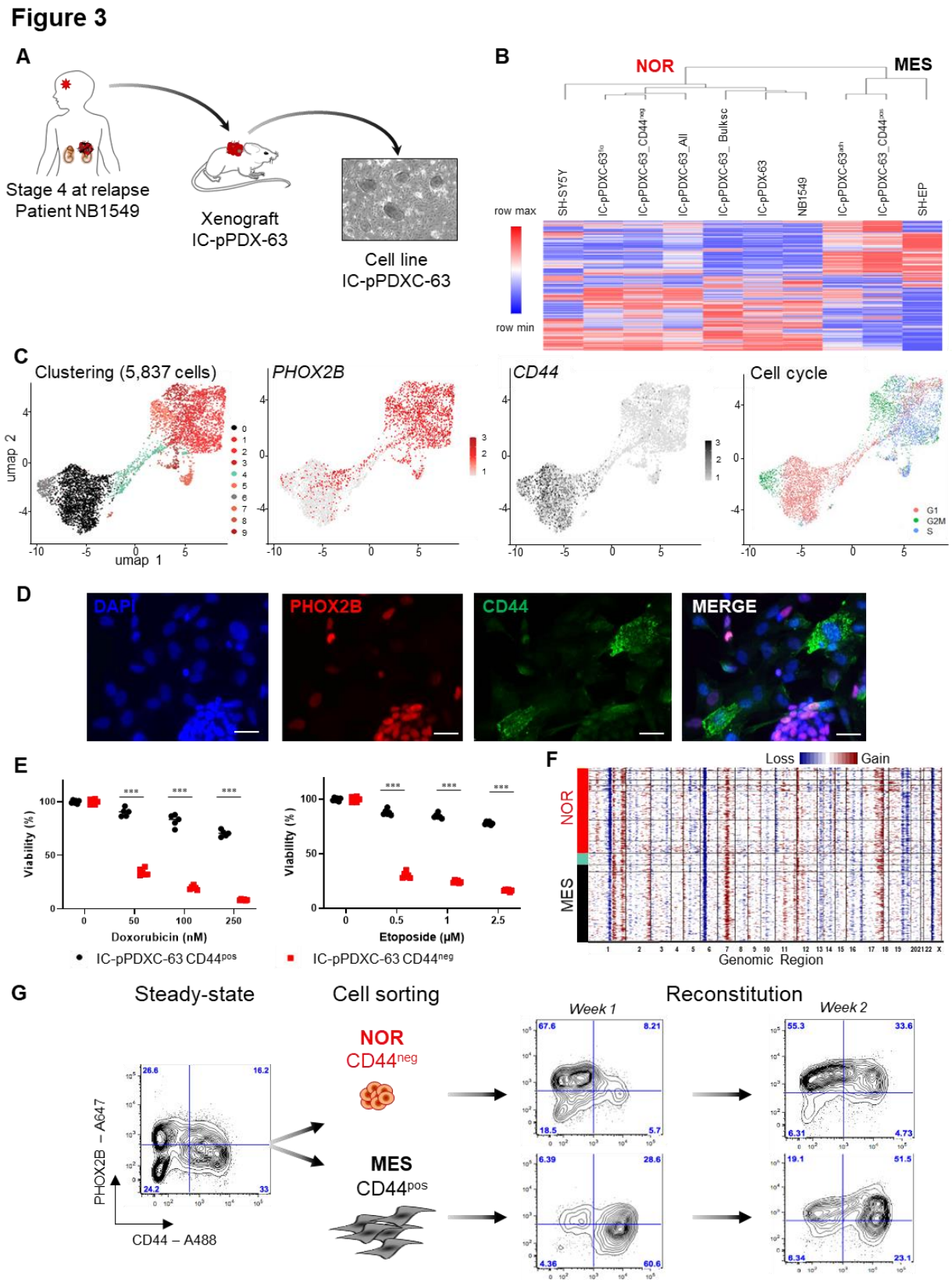

Figure 3. The IC-pPDXC-63 model exhibits a phenotypic plasticity between noradrenergic and mesenchymal identities. (**A**) *Ex vivo* culture of the noradrenergic IC-pPDX-63 neuroblastoma model includes floating neurospheres and adherent cells. (**B**) Unsupervised clustering using the top 10% of

genes with the highest IQR (Inter-Quartile Range) shows that the transcriptomic profile of the IC-pPDX-63 model and its derived-cell line (IC-pPDXC-63) are highly similar to that of the patient's tumor (NB1549) from which it has been generated. (**C**) Single-cell transcriptomic analyses by Seurat highlight both noradrenergic and mesenchymal clusters in the IC-pPDXC-63 cell line together with a bridge in-between. Four umap plots are shown (from left to right): the cell clustering, *PHOX2B* expression marking noradrenergic cells, *CD44* expression marking mesenchymal cells and the cell cycle. (**D**) Immunofluorescence shows the specific expression of the PHOX2B and CD44 markers by neurospheres and adherent cells, respectively (scale bar = 20 µm). (**E**) Mesenchymal (IC-pPDXC-63 $CD44^{pos}$) cells are more resistant to chemotherapy than noradrenergic (IC-pPDXC-63 $CD44^{neg}$) cells. Cell viability was measured with resazurin assay after 72 hours of chemotherapy treatments ((Doxorubicin 50, 100, 250 nM and Etoposide 0.5, 1, 2.5 µM)) (mean ± sd.; n = 6 replicates). P-values were determined via two-tailed unpaired Welch's t-test (**: $p<0.01$; ***: $p<0.001$). (**F**) Inferred genomic profile of the IC-pPDXC-63 cell line obtained with InferCNV on single-cell data. (**G**) Plasticity properties of the IC-pPDXC-63 cell line. $CD44^{pos}$ and $CD44^{neg}$ cells were FACS sorted and put back in culture. Each sorted population reconstituted a heterogeneous cell population after several days in culture.

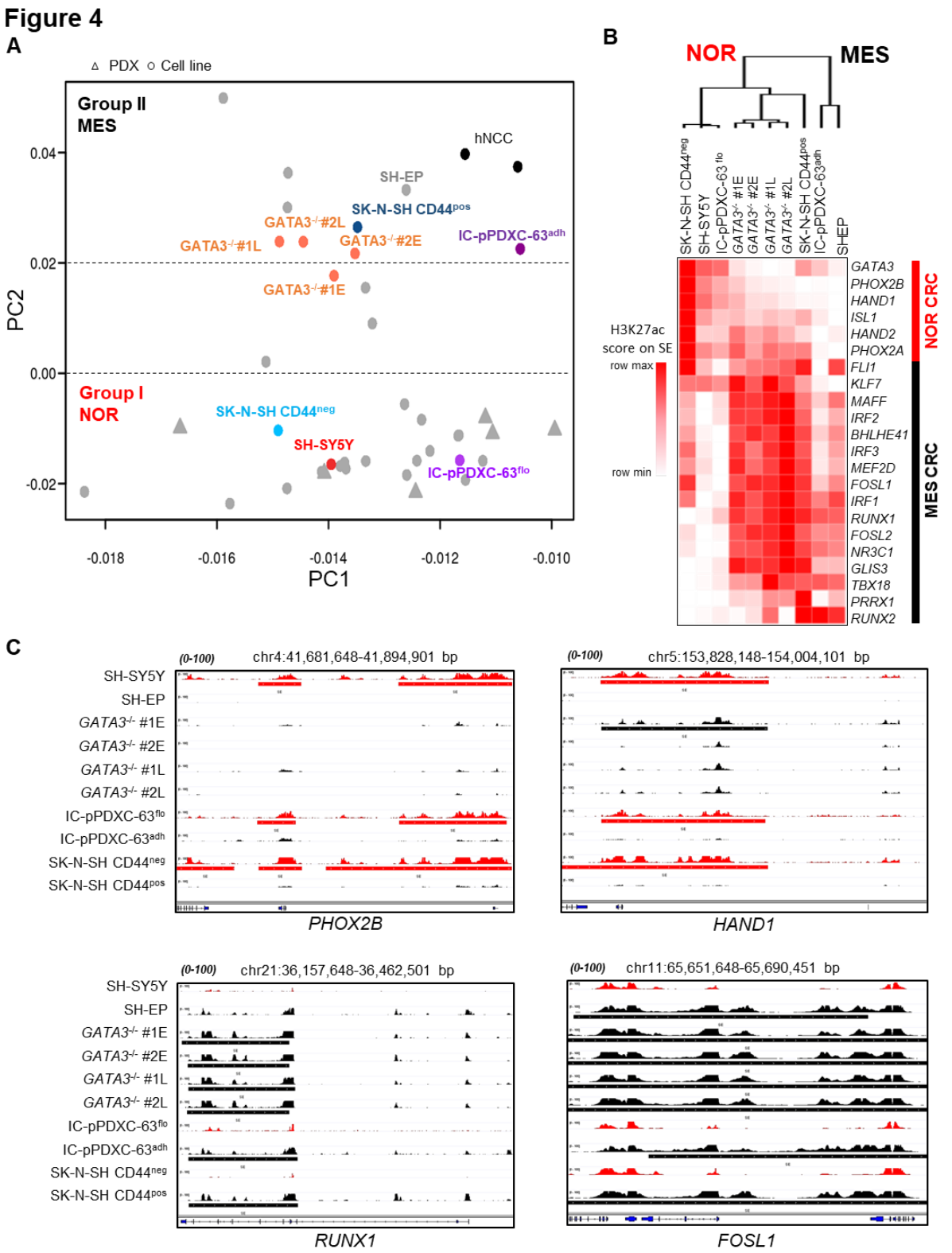

427

428 **Figure 4. Phenotypic plasticity relies on epigenetic reprogramming.** (**A**) Principal Component Analysis
429 (PCA) based on neuroblastoma and hNCC super-enhancer log scores[12] that discriminates the two
430 neuroblastoma cell groups I (noradrenergic-NOR) and II (NCC-like/mesenchymal-MES) and in which
431 were added the two *GATA3*$^{-/-}$ clones at early (E) and late (L) time points as well as the floating and

adherent cells of the IC-pPDXC-63 and CD44^{neg} and CD44^{pos} sorted cells of the SK-N-SH cell lines. (**B**) Heatmap showing the H3K27ac signal on the super-enhancer regions of the TFs of the noradrenergic (NOR) and mesenchymal (MES) CRC in the two *GATA3*$^{-/-}$ at both early (E) and late (L) time points, in floating and adherent cells of the IC-pPDXC-63 cell line and in the CD44^{pos} and CD44^{neg} sorted cells of the SK-N-SH cell line, and the SH-SY5Y and SH-EP control cell lines. For the TFs associated with several super-enhancers, the signal was summarized as described in the Methods section to have one value per TF. The unsupervised hierarchical clustering based on H3K27ac signals discriminated noradrenergic and mesenchymal TFs and cell identity. (**C**) Tracks of ChIP-seq profiles for H3K27ac at *PHOX2B, HAND1, RUNX1,* and *FOSL1* super-enhancers in the SH-SY5Y, SH-EP, the 4 *GATA3*$^{-/-}$ samples (2 at early (E) and 2 at late (L) time-points), the floating and adherent IC-pPDXC-63 cells and the CD44^{pos} and CD44^{neg} sorted SK-N-SH cells.

Figure 5

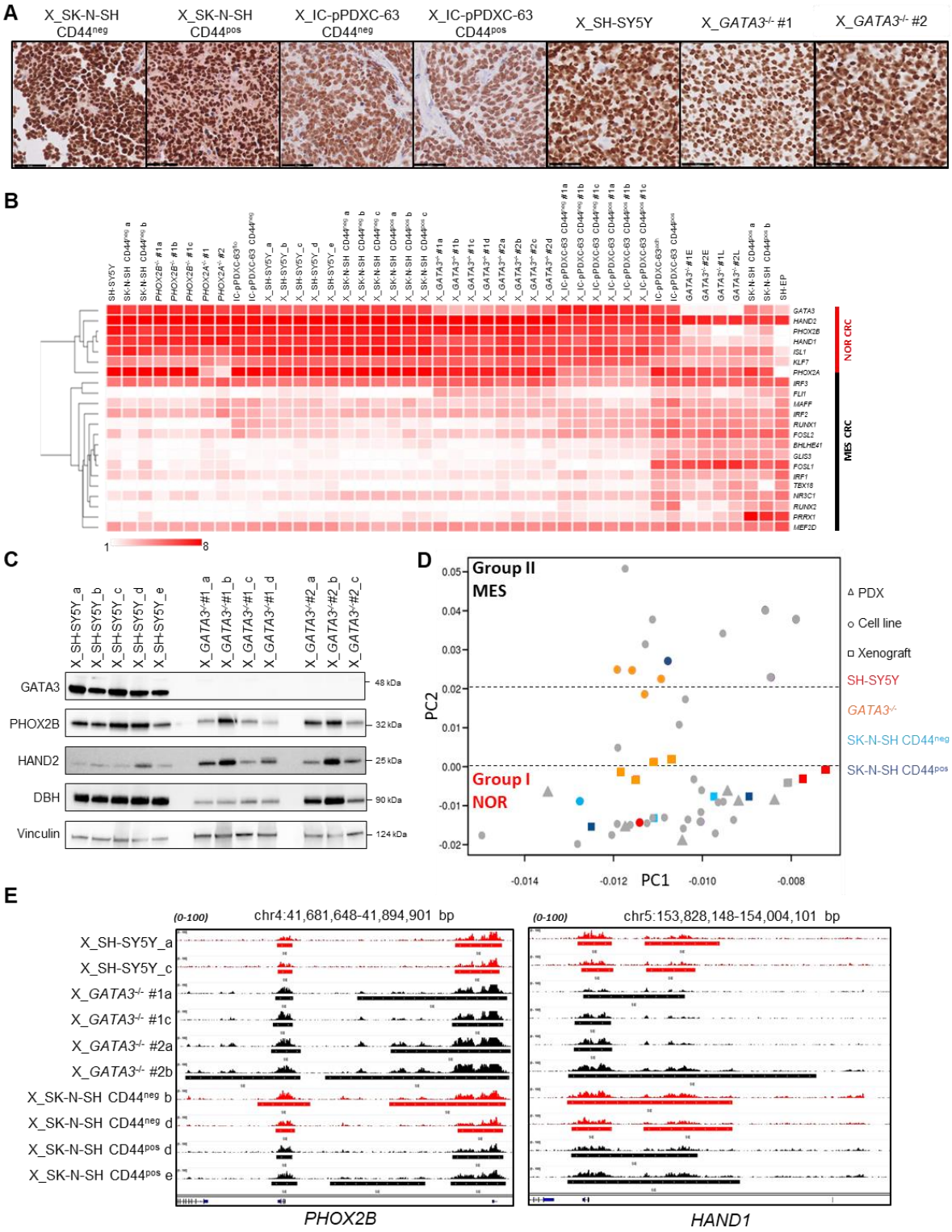

Figure 5. All sorted mesenchymal cells from the 3 models, SK-N-SH and IC-pPDXC-63 cell lines and *GATA3*$^{-/-}$ cells, adopt a noradrenergic identity when engrafted in mouse. (**A**) PHOX2B immunohistochemistry of one representative mouse xenograft per group (CD44^{neg} or CD44^{pos} sorted cells of SK-N-SH and IC-pPDXC-63 cell lines, SH-SY5Y control cells and *GATA3*$^{-/-}$ clones #1 and #2). Scale

bar = 50 µm. Similar results were obtained for all analyzed xenografts. (**B**) Heatmap showing the expression of the TFs associated with the noradrenergic or mesenchymal identity[12] reveals that all mouse xenografts exhibit a noradrenergic transcriptomic profile. (**C**) Western-blot analysis of GATA3, PHOX2B, HAND2 and DBH in the SH-SY5Y (n=5) and *GATA3*$^{-/-}$ clone xenografts (*GATA3*$^{-/-}$#1: n=4; *GATA3*$^{-/-}$#2: n=3) with Vinculin as a loading control. (**D**) PCA as in **Figure 4A** in which were added the xenografts of the SH-SY5Y and *GATA3*$^{-/-}$ clones and the CD44^{pos} or CD44^{neg} sorted cells of the SK-N-SH cell line. (**E**) Tracks of ChIP-seq profile for H3K27ac at *PHOX2B* and *HAND1* super-enhancers in the xenografts of the following cells: SH-SY5Y, *GATA3*$^{-/-}$ clones and SK-N-SH cell populations sorted according to CD44 expression.

Figure 6

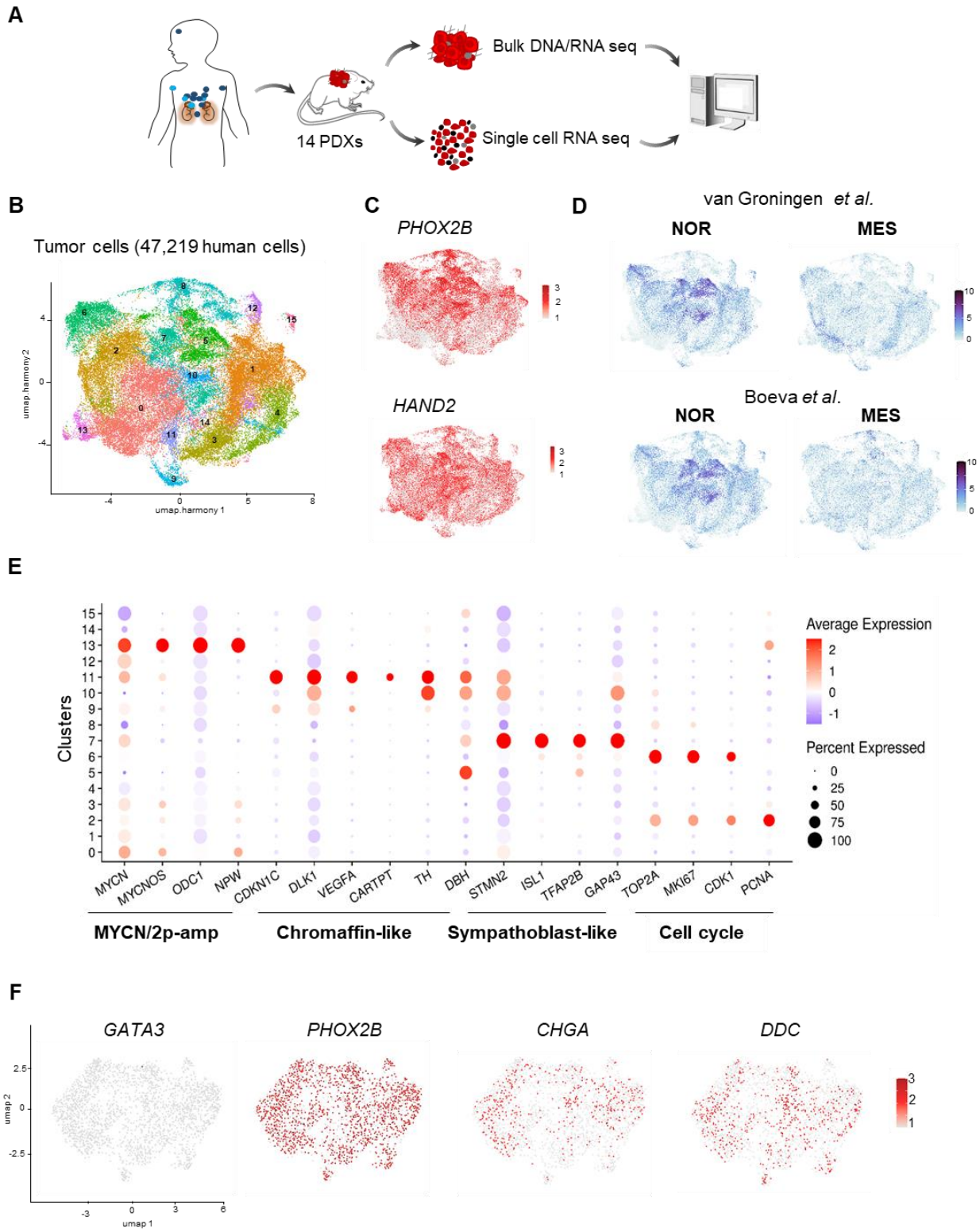

Figure 6. Single-cell transcriptomic analyses of 14 PDX models. (**A**) Schematic illustration of the overall procedure. scRNA-seq was performed for 14 neuroblastoma PDX models obtained either at diagnosis (light blue) or at relapse (dark blue) after tumor cell dissociation. In parallel, CNV profiles and global transcriptomes were established from the DNA and RNA of the bulk of the tumor. (**B**) Uniform manifold

464 approximation and projection (umap) of the 47,219 human cells obtained after the integration by
465 Harmony of the 14 PDX models. (**C**) *PHOX2B* and *HAND2* expression within the noradrenergic tumor
466 cells. (**D**) Plots of published noradrenergic (NOR) and mesenchymal (MES) signatures[12,13]. (**E**) Dot plot
467 graph illustrating cluster-specific gene expression. Four main populations of tumor cells could be
468 defined. (**F**) The GR-NB7 PDX model does not express *GATA3* but exhibits a noradrenergic phenotype
469 as shown by the plot of *PHOX2B*, *CHGA* and *DDC* expression in the scRNAseq data.

MATERIAL AND METHODS

RESOURCE AVAILABILITY

Lead Contact

Further information and request for resources should be directed to and will be fulfilled by the Lead Contact, Isabelle Janoueix-Lerosey (isabelle.janoueix@curie.fr).

Material availability

Availability of the IC-pPDXC-63 model generated in this study is subjected to a Material Transfer Agreement.

Data and code availability

ChIP-seq (RRID:SCR_001237) data of cell lines and xenografts (34 samples) are available in Gene Expression Omnibus (GEO, RRID:SCR_005012) under the accession number GSE154907.
All single-cell RNA-seq from PDXs, all RNA-seq and the ChIP-seq data on the IC-pPDXC-63 cell line are available in European Genome-Phenome Archive (EGA) under the accession number EGAS00001004781 (ongoing submission).

EXPERIMENTAL MODELS

Neuroblastoma cell lines

The SK-N-SH (Cat# HTB-11, RRID:CVCL_0531) and SH-SY5Y (Cat# CRL-2266, RRID:CVCL_0019) cell lines have been obtained from the ATCC. The SH-EP cell line has been kindly provided by M. Schwab. Cell line authentication was done by STR profiling with PowerPlex® 16 HS System from Promega. The IC-pPDXC-63 cell line was derived from the IC-pPDX-63 model. *GATA3*$^{-/-}$ clones were genetically modified from the SH-SY5Y cell line. Cells were grown at 37°C with 5% CO_2 in a humidified atmosphere in DMEM/HIGH glucose (Cat# SH30022.01, GE Healthcare) for SK-N-SH, SH-SY5Y and *GATA3*$^{-/-}$ clones and in RPMI-1640 (Cat# SH30027.01, GE Healthcare) for IC-pPDXC-63 and SH-EP cell lines, with 10% FBS (Cat# SV30160.03, GE Healthcare). Cells were monthly checked by qPCR (Venor® GeM qEP 11-9250, Minerva biolabs®) for the absence of mycoplasma.

Mouse xenograft experiments

For each cell line, 5 million cells were injected subcutaneously in the flanks of 8 week-old Nude or NSG mice with a ratio of 50/50 standard medium (DMEM: Cat# SH30022.01, GE Healthcare) and BD Matrigel™ (Cat# 356234, BD Biosciences). Tumor volume was measured every 2 or 3 days with a

caliper. Mice were sacrificed when the tumor reached a volume of 2,000 mm^3 calculated as V = (a/2) * b * ((a+b)/2), a and b being the largest and smallest diameters, respectively.

In vivo experiments for this study were performed in accordance with the recommendations of the European Community (2010/63/UE) for the care and use of laboratory animals. Experimental procedures were specifically approved by the ethics committee of the Institut Curie CEEA-IC #118 (Authorization APAFIS#11206-2017090816044613-v2 given by National Authority) in compliance with the international guidelines.

Patient-derived Xenografts (PDX models)

Written informed consents for the establishment of PDXs were obtained for all patients from parents or guardians. GR-NB4 (previously named MAP-GR-A99-NB-1[12]), GR-NB5 (previously named MAP-GR-B25-NB-1[12]), GR-NB7 and GR-NB10 have been provided by Birgit Geoerger (Gustave Roussy, Villejuif, France). IC-pPDX-63, IC-pPDX-75, IC-pPDX-109 and IC-pPDX-112 have been developed at Institut Curie. HSJD-NB-003, HSJD-NB-004, HSJD-NB-005, HSJD-NB-007, HSJD-NB-009 and HSJD-NB-011 PDX models have been provided by Angel Carcaboso (Institut de Recerca San Joan de Déu, Barcelona, Spain). These models have been generated from patients under an Institutional Review Board-approved protocol or within a clinical trial, respectively (**Table S2**).

METHOD DETAILS

CRISPR-Cas9 KO strategy

The guide RNAs used to specifically target the *PHOX2A*, *PHOX2B* and *GATA3* genes were selected from the CRISPOR website (crispor.tefor.net) for their high predicted efficiency and specificity: CAATTCGTACGACTCGTGCG and CTTGGAATCGTCGTCCTCGG targeting *PHOX2A*, CCCAGCCATACAGGACTCGT and AAACTCTTCACGGACCACGG targeting *PHOX2B*, GTACTGCGCCGCGTCCATGT and GAGCTGTACTCGGGCACGTA targeting *GATA3*. *PHOX2A, PHOX2B* and *GATA3* KO were performed by inducing a large deletion between exons 1 and 3, exons 1 and 2 or exons 2 and 3, respectively (**Figure S1A**). To screen the KO clones, 3 pairs of primers were used per gene: surrounding the deleted region (*PHOX2A*: 5'-CCGATGGACTACTCCTACCTC-3', 5'-GCCGGCAGCTAGAAGAGATT-3', *PHOX2B*: 5'-GTTGGACAGCTCAGTTCCC-3' , 5'-CCCTAGGTCCTTCTCACTCG-3', *GATA3*: 5'-GCAGAATTGCAGAGTCGTCG-3', 5'-AAGAGCTGGCTCCTACCTGT-3'), at the 1st cut site (*PHOX2A*: 5'-GGCCGATGGACTACTCCTACCT-3', 5'-GGGGGACAGTCGCATTCAC-3', *PHOX2B*: 5'-CAGCAATAAGACCAACCGCT-3', 5'-GGTTCGGGTGTGACTAGGAT-3', *GATA3*: 5'-TTGCTAAACGACCCCTCCA-3', 5'-AAATGAACCAGGAACGGCAG-3') and at the 2nd cut site (*PHOX2A*: 5'-AGCTTTGAAAACCCGGAGCC-3', 5'-CGGCTGCCAAGCCTTAAGTA-3', *PHOX2B*: 5'-TCTCAAGTCCGTCACATCGC-3', 5'-

539 ATTTCTGATCGGCCATGGGG-3', *GATA3*: 5'-TGCGAGGTAGAGATTCCCCA-3', 5'-
540 GCTAGGATGGGAGGACATGC-3'). The guide RNAs, crRNA and the recombinant Cas9 protein were
541 purchased from Integrated DNA Technologies. Their reconstitution, assembly and delivery to the cells
542 were performed following manufacturer's instructions. KO efficiency was determined 2 days after cell
543 transfection and clones were generated by plating 200 cells in 10 cm culture dishes. KO clones were
544 verified by Sanger sequencing with the BigDye Terminator V1.1 Cycle Sequencing Kit (130-098-462,
545 Thermo Fisher).
546
547 **Phalloidin staining**
548 100,000 cells for SH-SY5Y, *PHOX2B*$^{-/-}$ and *PHOX2A*$^{-/-}$ clones, 50,000 cells for *GATA3*$^{-/-}$ clones were plated
549 in a 4-well Lab-Tek chamber (Cat# 177399PK, Thermo Fisher) 24 hours before immunostaining. Cells
550 were fixed with 4% PFA buffer, permeabilized with a 0.2% triton solution and blocked in a 1% BSA 0.1%
551 triton solution. Phalloidin–Tetramethylrhodamine B isothiocyanate (Sigma Aldrich Cat# P1951,
552 RRID:AB_2315148) was used at 1:100 to stain actin filaments. DAPI (Cat# 62248, Thermo Fisher) was
553 diluted at 1: 1,000 in ProLong™ Gold (Cat# P36930, Thermo Fisher).
554
555 **Immunoblotting**
556 Proteins were extracted using a RIPA buffer (NaCl 150m M, Tris 50 mM pH=7.5, EDTA 1 mM, SDS 0.1%,
557 deoxycholic acid 0.25%, IGEPAL 1%, PMSF 1 mM) supplemented with protease inhibitor cocktail tablets
558 (Cat# 11836145001, Roche). 30 to 40 µg of proteins were used for Western blot analysis. The
559 antibodies targeting the PHOX2B N-terminal part (Santa Cruz Biotechnology Cat# sc-376997,
560 RRID:AB_2813765), PHOX2A (Santa Cruz Biotechnology Cat# sc-81978, RRID:AB_1127226) and DBH
561 (Santa Cruz Biotechnology Cat# sc-15318) were used at 1:500. Anti-GATA3 (Cell Signaling Technology
562 Cat#5852) and HAND2 (Abcam Cat# ab200040) were used at 1: 1,000 and anti-Vinculin (Abcam Cat#
563 ab129002, RRID:AB_11144129) was used at 1: 10,000.
564
565 **Proliferation assays**
566 To evaluate the proliferation rate of the *PHOX2B*$^{-/-}$ and *GATA3*$^{-/-}$ clones compared to the parental SH-
567 SY5Y cell line, 10,000 cells were plated in a 24-well plate in 6 replicates. Cells were then counted at day
568 3, 7 and 10, using a Vi-cell XR Viability Analyzer (Beckman Coulter).
569
570 **Invasion and migration assays**
571 Invasion assays were performed in 96-well low adherent plates (Corning) with 2,000 cells per well for
572 the SH-EP cell line (n=12), and 10,000 cells per well for the SH-SY5Y cell line (n=12) and *GATA3*$^{-/-}$ clones
573 (n=18). After 4 days of culture, spheroids were embedded in Corning® Collagen I (cat# 354249, Corning)

and cultured in normal conditions. Invasive cells were observed 72 hours after spheroid inclusion and the area of migration was quantified using the ImageJ software (RRID:SCR_003070).

Transwell experiments were performed using 12-well 8 µm culture inserts (Dutscher). 50,000 cells were used per condition. After 24 hours of incubation, cells that have migrated through the insert membrane were fixed and stained with crystal violet (Sigma Aldrich). In each replicate, migrated cells were quantified using the mean of 6 different images, 6 replicates were performed per cell line.

Immunofluorescence

100,000 cells for SK-N-SH and IC-pPDXC-63 cell lines were plated in a 4-well Lab-Tek chamber (Cat# 177399PK, Thermo Fisher) 48 hours before immunostaining. Cells were fixed with 4% PFA buffer, permeabilized with a 0.2% triton solution and blocked in a 1% BSA 0.1% triton solution and incubated with anti-PHOX2B (Santa Cruz Biotechnology Cat# sc-376997, RRID:AB_2813765) and anti-CD44 (Cat# 15675-1-AP, Proteintech) at 1:100. Secondary antibodies were Cy5-Anti-Mouse (Cat# 715-175-151, Jackson ImmunoResearch Labs / 1:100, RRID:AB_2340820) and Cy3-Anti-Rabbit (Cat# 711-165-152, Jackson ImmunoResearch Labs / 1:100, RRID:AB_2307443) and DAPI (Cat# 62248, Thermo Fisher) was diluted at 1: 1,000 in ProLong™ Gold (Cat# P36930, Thermo Fisher).

Chemotherapy treatments

SH-SY5Y, SH-EP or *GATA3*$^{-/-}$ clones were plated in a 24-well plate 24 hours before the chemotherapy treatments. Seeding densities for each cell lines were optimized to reach 80% confluence in the untreated cells. Cells were treated with 3 different doses of the conventional chemotherapy for 2 days and cell viability was assessed using a Vi-cell XR Viability Analyzer (Beckman Coulter); 6 replicates were performed for each cell line and each dose.

IC-pPDXC-63 and SK-N-SH cell lines were plated in 96-well plates 24 hours before the addition of doxorubicin or etoposide. Seeding densities for each cell line were optimized to reach 80% confluence in the untreated cells. Cells were treated with chemotherapeutic agents for 72 hours. Cell viability was then measured using the Resazurin reagent (Sigma-Aldrich).

RNA-sequencing and analyses

RNAs were extracted from frozen tumors by mechanical crushing followed by TRIzol® reagent (Cat#15596018, Invitrogen) and purified with the NucleoSpin RNA kit (Cat# 740955.50, Macherey-Nagel). For the bulk scRNA-seq samples and the cell lines, extraction and purification were done directly using this NucleoSpin RNA kit. RNA quality was assessed with a Bioanalyzer instrument and RNAs with an RNA Integrity Number above 7 were processed for sequencing as previously described[12]. RNA sequencing libraries were prepared from 500 ng to 1 µg of total RNA using the Illumina TruSeq

609 Stranded mRNA Library preparation kit according to manufacturer recommendation. For the
610 xenografts of IC-pPDXC-63 *in vivo* sample, mRNA Library preparation was done with TruSeq RNA Exome
611 from Illumina. 100 bp paired-end sequencing was performed with the Illumina NovaSeq 6000
612 instrument (pair-ended, 100 nt).
613 Reads were aligned to the human reference genome hg38/GRCh38 using STAR 2.6.1a_08-27
614 (RRID:SCR_015899, https://github.com/alexdobin/STAR) with the following options: -
615 outFilterMismatchNoverLmax 0.04 --alignIntronMin 20 – lignIntronMax 1000000 –
616 outFilterMultimapNmax 20. Gene expression values (FPKM=fragments per kilobase per million reads)
617 were computed by Cufflinks v2.2.146 (RRID:SCR_014597, http://cole-trapnell-lab.github.io/cufflinks/)
618 and further normalization between samples was done using quantile normalization (R/Bioconductor
619 package LIMMA (RRID:SCR_010943)).
620
621 **PHOX2B immunohistochemistry**
622 Tumors were fixed in a 4% formol buffer (VWR) during 24 hours, embedded in paraffin and cut in 4 µm
623 slices. For PHOX2B immunohistochemistry, the REAL™ EnVision™ Detection System (Cat# K406511-2,
624 Agilent Technologies) was used and the antibody against PHOX2B (Cat# sc-376997, Santa Cruz) was
625 diluted at 1:200. Xenograft slices were also colored with a hematoxylin solution.
626
627 **ChIP-seq and analyses**
628 H3K27ac chromatin immunoprecipitation (ChIP) experiments were performed as previously
629 described[12] using the iDeal ChIP-seq kit for histones (Cat# C01010171, Diagenode) and the H3K27ac
630 rabbit polyclonal antibody (Abcam Cat# ab4729, RRID:AB_2118291). Illumina sequencing libraries
631 were prepared from the ChIP and input DNA and sequenced on the Illumina NovaSeq 6000 instrument
632 (single reads, 100 nt). ChIP-seq reads were mapped to the human reference genome hg19/GRCh37
633 using Bowtie2 v2.1.0 (http://bowtie-bio.sourceforge.net/bowtie2/index.shtml) and further analyzed
634 with HMCan v1.40 (RRID:SCR_010858)[45]. Super-enhancers were called with LILY software as previously
635 described[12]. LILY was also used to normalize HMCan density profiles between samples. The H3K27ac
636 signal on super-enhancers shown in the heatmap was computed as the sum of normalized H3K27ac
637 densities divided by the length of the super-enhancers. For TF genes associated with several super-
638 enhancers, the signal of the associated super-enhancers is summed and divided by their total length.
639 PCA was computed as described previously[12].
640
641 **Flow cytometry and sorting**
642 Flow cytometry analysis was performed with the BD™ LSRII cytometer. Cells were detached with
643 TrypLE™ Express Enzyme (Cat# 12604013, Gibco), suspended in PBS and permeabilized with the

644 IntraPrep kit (Cat# A07803, BeckmanCoulter). The cell suspension was incubated with PHOX2B [Clone
645 B-11] - AlexaFluor® 647 (Cat# SC-376997 AF647, Santa Cruz) and CD44-FITC (Cat# 103005, Biolegend,
646 RRID:AB_312956) antibodies during 40 min at 4°C.
647 Flow cytometry sorting was performed with the S3e™ cell sorter (Bio Rad). Cells were detached with
648 TrypLE™ Express Enzyme (Cat# 12604013, Gibco), suspended in PBS and incubated with CD44-FITC
649 antibody 30 min at 4°C in dark. Cells positive and negative for CD44 staining were sorted.
650 The first gating based on FSC/SSC represents 60% for IC-pPDXC-63 and 75% for SK-N-SH. Doublet cells
651 are eliminated by gating on SSC-W / SSC-H followed by FSC-W / FSC- H. The second gating based on
652 DAPI negative staining eliminates dead cells. The boundaries between positive staining and negative
653 staining are always more than 1 Log of fluorescence intensity. A control tube without staining is always
654 analyzed to determine auto-fluorescence.
655
656 **Tumor dissociation into single-cell suspension**
657 PDX tumors were cut with scalpels in small fragments. Enzymatic dissociation was realized in CO_2
658 independent medium (GIBCO) containing 150 µg/mL Liberase™ TL Research Grade (Cat# 5401020001,
659 Merk) and 150 µg/mL DNase (DN25, Sigma Aldrich), for 30 min at 37°C with 400 rpm agitation. Cell
660 suspension was then filtered using 70 µm cell strainer (Cat# 130-098-462, Miltenyi Biotec). The cell
661 suspension was washed twice with PBS. Viability was measured using Vi-cell XR Viability Analyzer
662 (Beckman Coulter). For some PDXs, the Mouse Cell Depletion KIT was used following the
663 manufacturer's instructions (Cat# 130-104-694, Miltenyi Biotec).
664
665
666 **Single-cell RNA-sequencing experiments and preprocessing of data**
667 Single-cell RNA-seq was performed with the 10x Genomics Chromium Single Cell 3' Kit (v3) according
668 to the standard protocol. Libraries were sequenced on an Illumina HiSeq2500 or NovaSeq 6000
669 sequencing platform.
670 CellRanger version 3.1.0 (10x Genomics, https://support.10xgenomics.com/) was used to demultiplex,
671 align and generate UMI count tables from sequencing reads. Two reference genomes were used to
672 align reads:
673 • The human reference genome (hg38/GRCh38) for *in vitro* cell lines.
674 • A human-mouse reference genome (GRCh38-mm10) for the 14 neuroblastoma PDX models. In this
675 scenario, we identified the mouse and human cells after inspection of the percentage of coverage from
676 GRCh38 genome. We labeled cells as either human (at least 80%), murine (less than 30%) or human-
677 murine doublets (between 30-80%). Only human and human-murine doublet cells were selected and
678 coverage plus gene information of only GRCh38 genome were retained for downstream analysis.

Summary of analyses are shown in **Table S3**. Of note, we performed two technical replicates for three models: HSJD-NB-005, IC-pPDX-63 and IC-pPDX-75 (* in Table S3) to assess reproducibility at distinct passages in mice (data not shown).

Doublet detection

Scrublet[46] v0.2.1 was used to detect potential doublets using default parameters (expected_doublet_rate=0.06). Cells marked as doublets were removed from subsequent analysis (results in **Table S3**). Doublet detection was only feasible on samples aligned to GRCh38 genome.

Quality control of single-cell data

First, all ribosomal genes (defined as *RLP/RPS* genes) were removed from the raw expression matrices. Then, coverage thresholds were set for each sample individually; an upper threshold was set to remove outlier cells with coverage greater than the 99th percentile, and a lower threshold was set to remove low quality cells with coverage inferior to the 1st percentile, except for the IC-pPDXC-63 cell line for which the limits were 1000 UMI and 500 genes detected per cell. To avoid cells with low number of genes, the same lower threshold was applied on the number of genes thus defining a minimum number of genes required. Finally, cells with more than 20% of reads mapping mitochondrial genes were removed.

Normalization of single-cell data

Raw UMI counts were normalized using the "SCTransform" function of Seurat[47,48] v3.1.5 (RRID:SCR_007322). Regressed variables included cell coverage, number of features, and the percentage of UMI from mitochondrial genes.

Dimensionality reduction and cluster identification

Normalized count data was subjected to dimensionality reduction keeping the first 30 principal components. Uniform Manifold Approximation and Projections (umap) embeddings were calculated using these PCs as input and cells were clustered using the "FindClusters" function of Seurat.

Cell type annotation

Marker genes that define cell clusters were identified after differential expression analysis using Seurat's "FindAllMarkers" function. Clusters were annotated by comparing their top marker genes to canonical cell type markers from the literature.

Generation of single-cell signature scores

To plot the expression of gene signatures in single cells, we used the "AddModuleScore" function from Seurat R package with 100 genes in the control gene set. Expression scale was binned into 10 bins when a gene signature is plotted and into 3 bins (1= low, 2= median, 3= high) when a single gene is plotted.

scRNA-seq data integrations

Harmony[24] (https://github.com/immunogenomics/harmony) was used to integrated the 14 PDX models. Downstream analysis was carried out as described in ''Dimensionality reduction and cluster identification". Of note, when several single-cell transcriptomes are available for the same model, only one was used for the integration to avoid over-representation.

Cell cycle analysis

We scored single cells based on expression of G2/M and S phase markers using Seurat's "CellCycleScoring" function.

Copy number analysis in single cells

Copy number variations at the single cell level were called with R package InferCNV v1.2.1 [22] (https://github.com/broadinstitute/inferCNV) using default parameters. Normal cells from the microenvironment were used as reference cells. Cells with fewer than 1000 UMI were excluded and monocytes from publicly available single cell RNA sequencing of healthy human PBMCs[49,50] (GEO: GSE115189) were used as reference cells (n=376).

QUANTIFICATION AND STATISTICAL ANALYSES

Statistical tests were performed using GraphPad Prism 8 (RRID:SCR_002798). Significance values are described in the figure legends. P-values were determined via two-tailed unpaired Welch's t-test (**:$p<0.01$; ***:$p<0.001$).

742 **SUPPLEMENTAL INFORMATION**
743

744 **Figure S1:** Knock-out of *PHOX2A, PHOX2B* and *GATA3* genes by CRISPR-Cas9.

745 **Figure S2:** Sorted mesenchymal cells from the IC-pPDXC-63, SK-N-SH and *GATA3*$^{-/-}$ cell lines, adopt a
746 noradrenergic identity when engrafted in the mouse.

747 **Figure S3:** Detailed analyses of single-cell RNAseq of the 14 PDX models.

748

749

750 **Table S1:** Expression levels of noradrenergic markers, TFs of the noradrenergic and mesenchymal CRCs
751 in cell lines and xenografts.

752 **Table S2:** Characteristics of the 14 neuroblastoma PDX models studied by scRNA-seq.

753 **Table S3:** Filtering of human cells with high quality data for the 14 neuroblastoma PDX models.

754 **Table S4:** Lists of genes that are up-regulated in the different clusters of noradrenergic cells in a series
755 of 14 neuroblastoma PDX models.

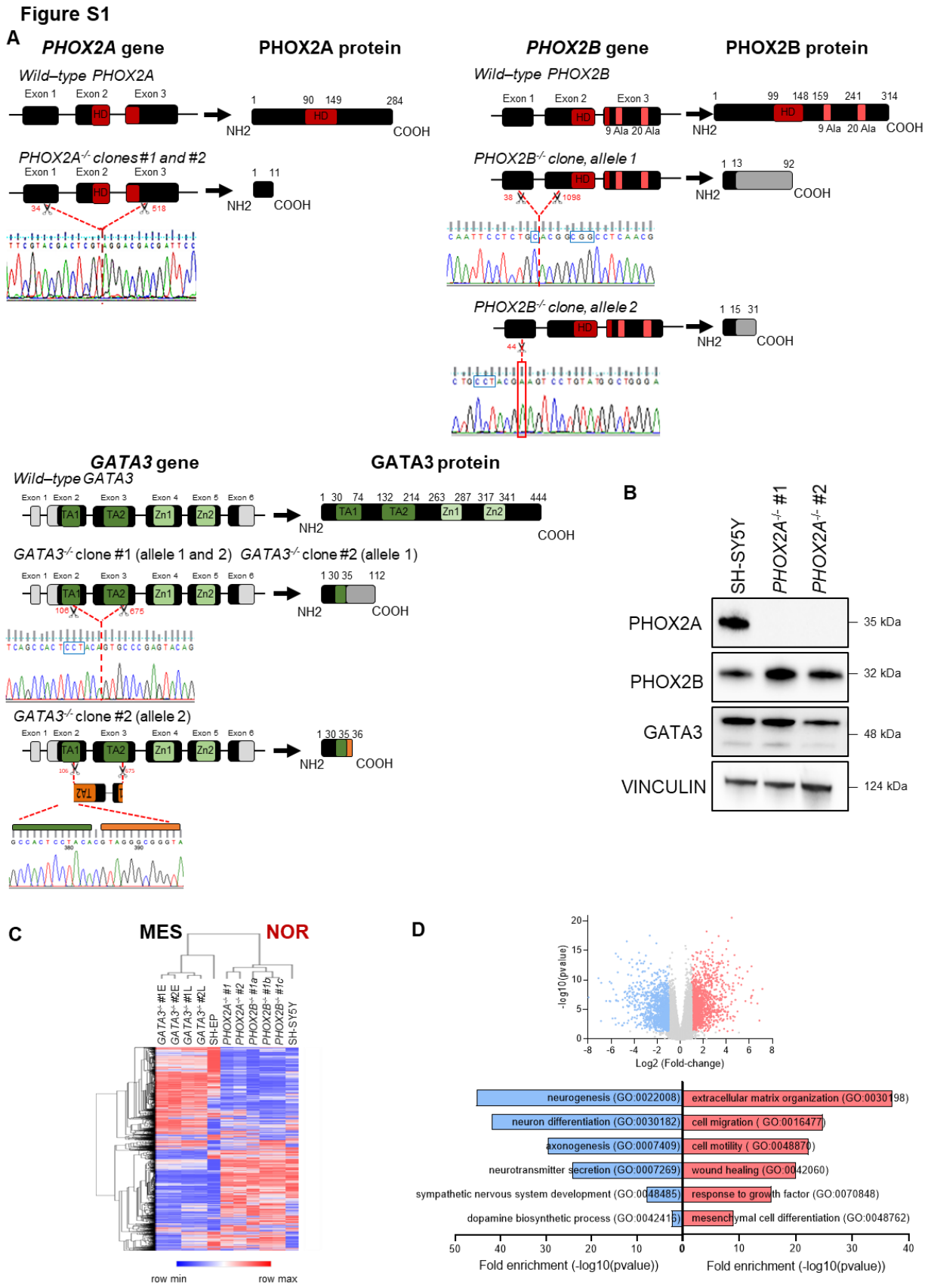

Figure S1: Knock-out of *PHOX2A, PHOX2B* and *GATA3* genes by CRISPR-Cas9. (**A**) Two guide RNAs were chosen per gene to induce large deletions (see Methods). The PAM motifs are surrounded in blue when still presents in the modified sequence. Both *PHOX2A*$^{-/-}$ clones are homozygous and present with

a large deletion between the 1st and 3rd exons, following Cas9-induced breaks at the expected positions. This results in a frameshift and subsequently in a truncated protein that has lost all its functional domains, containing only the 11 first amino acids of the normal PHOX2A protein. The *PHOX2B*$^{-/-}$ clone is heterozygous. In the first allele, the Cas9 induced one break in exon 1 in the PAM motif instead of 3 bp upstream and one break in exon 2, 4 bp upstream of the PAM (instead of 3 bp upstream). This results in a frameshift and subsequently in a truncated protein, in which only the first 13 amino acids of the normal PHOX2B protein are conserved. In the second allele, the Cas9 induced only one cleave in the first exon, 3 bp upstream of the PAM, as expected and an "A" insertion was observed. This results in a frameshift and subsequently in a truncated protein, in which only the first 15 amino acids of the normal PHOX2B protein are conserved. *GATA3*$^{-/-}$ clone #1 is homozygous and presents with a large deletion between the 2nd and 3rd exons, following Cas9-induced breaks that occurred at the expected positions. This leads to a truncated protein of 112 amino acids that has lost all its functional domains and contains only the 35 first amino acids of the normal GATA3 protein. *GATA3*$^{-/-}$ clone #2 is heterozygous. One allele is similar to those of *GATA3*$^{-/-}$ clone #1. For the second allele, the break occurred at the expected position but the *GATA3* sequence between these two cleavage sites was reintegrated in the reverse direction, with one "C" insertion. This results in the translation of an aberrant protein of 36 amino acids, which contains only the first 35 amino acids of the normal GATA3 protein (HD: homeodomain, Ala: poly-alanines track, TA: transactivation domain, Zn: zinc finger domain) (**B**) Western blot analysis of PHOX2A, PHOX2B and GATA3 TFs in the 2 *PHOX2A*$^{-/-}$ clones and in the SH-SY5Y cell line, Vinculin was used as a loading control. (**C**) Unsupervised clustering analysis using the top 10% of genes with the highest IQR (inter-quantile range) shows that *PHOX2A*$^{-/-}$ and *PHOX2B*$^{-/-}$ clones resemble the parental noradrenergic SH-SY5Y cell line whereas *GATA3*$^{-/-}$ clones are clustered in the same branch as the SH-EP mesenchymal cell line. (**D**) Volcano plot of a differential analysis comparing the 4 *GATA3*$^{-/-}$ samples with 5 noradrenergic neuroblastoma cell lines without *MYCN* amplification (CLB-GA, NB-EBc1, SH-SY5Y, SJNB-1 and SK-N-FI). We used a raw p-value <0.05 and a fold-change >2. Gene Ontology analysis using ToppGene (https://toppgene.cchmc.org/enrichment.jsp) performed on the lists of differentially expressed genes in the *GATA3*$^{-/-}$ samples compared to the other neuroblastoma cell lines.

Figure S2

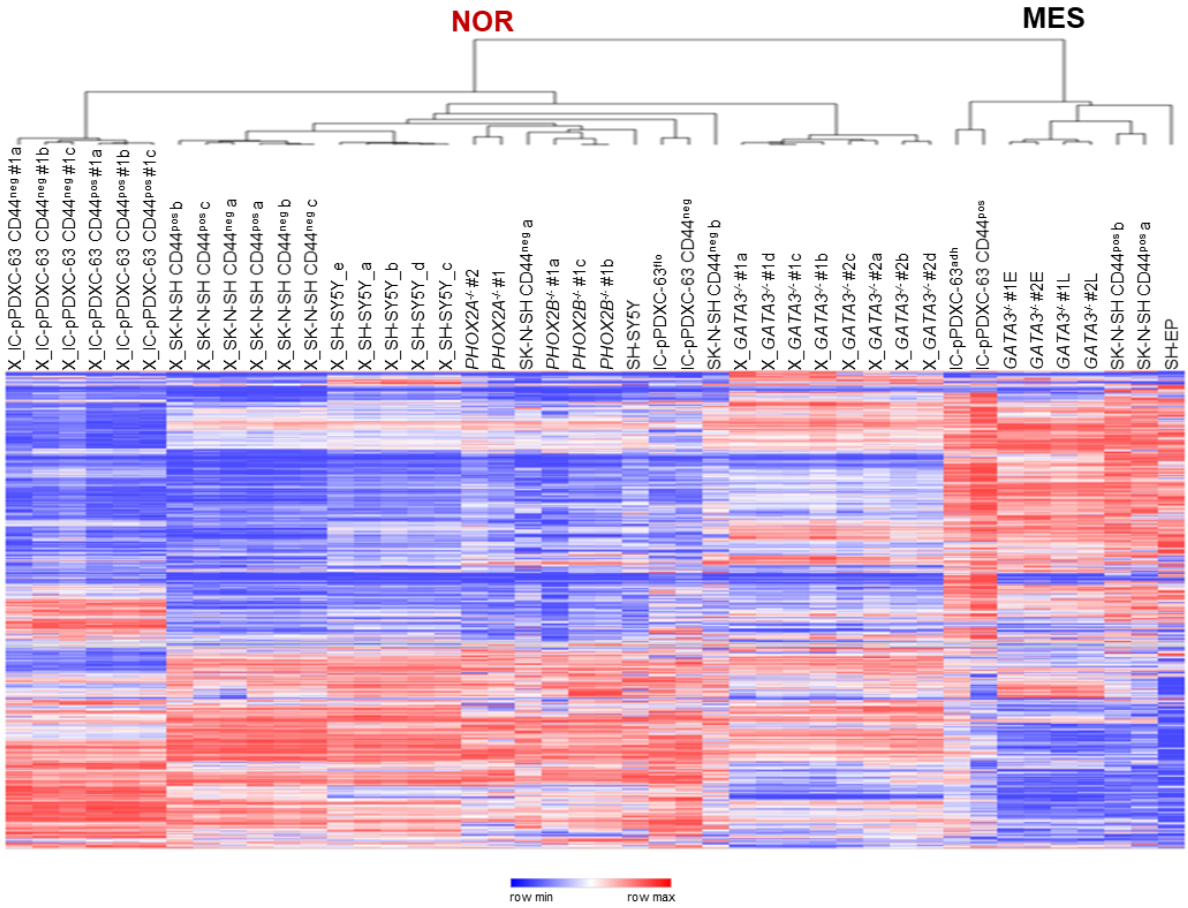

Figure S2: Sorted mesenchymal cells from the IC-pPDXC-63, SK-N-SH and *GATA3*$^{-/-}$ cell lines, adopt a noradrenergic identity when engrafted in the mouse. Unsupervised hierarchical clustering based on a transcriptomic signature[13] discriminating noradrenergic and mesenchymal cells shows that all the *in vitro* mesenchymal cell populations engrafted in mice give tumors with a noradrenergic transcriptomic profile.

Figure S3

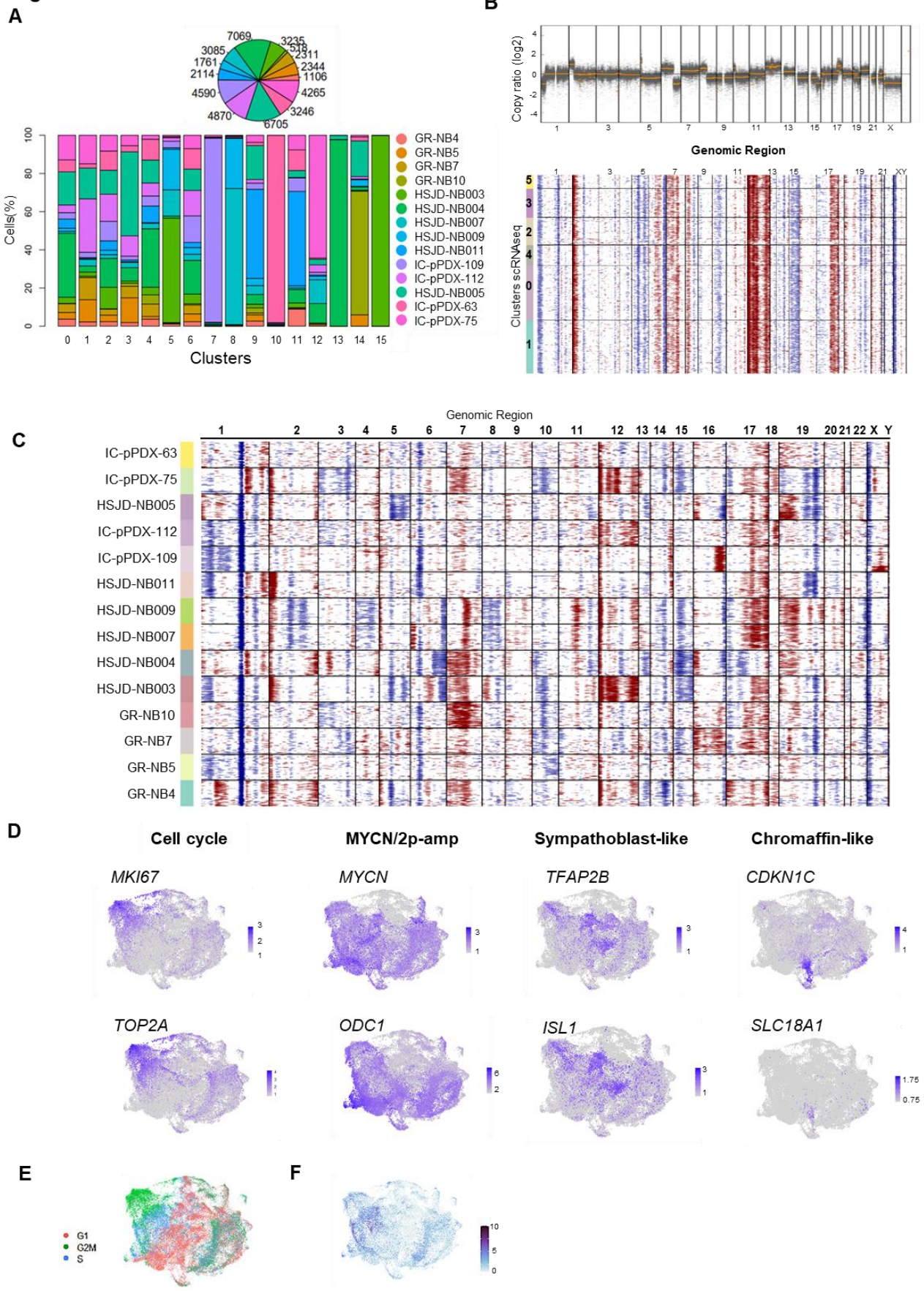
A
7069
3235
538
2311
2344
1106
4265
3246
6705
4870
4590
2114
1761
3085
Cells(%)
Clusters
GR-NB4
GR-NB5
GR-NB7
GR-NB10
HSJD-NB003
HSJD-NB004
HSJD-NB007
HSJD-NB009
HSJD-NB011
IC-pPDX-109
IC-pPDX-112
HSJD-NB005
IC-pPDX-63
IC-pPDX-75
B
Copy ratio (log2)
Genomic Region
Clusters scRNAseq
C
Genomic Region
IC-pPDX-63
IC-pPDX-75
HSJD-NB005
IC-pPDX-112
IC-pPDX-109
HSJD-NB011
HSJD-NB009
HSJD-NB007
HSJD-NB004
HSJD-NB003
GR-NB10
GR-NB7
GR-NB5
GR-NB4
D
Cell cycle
MYCN/2p-amp
Sympathoblast-like
Chromaffin-like
MKI67
MYCN
TFAP2B
CDKN1C
TOP2A
ODC1
ISL1
SLC18A1
E
G1
G2M
S
F

Figure S3

G

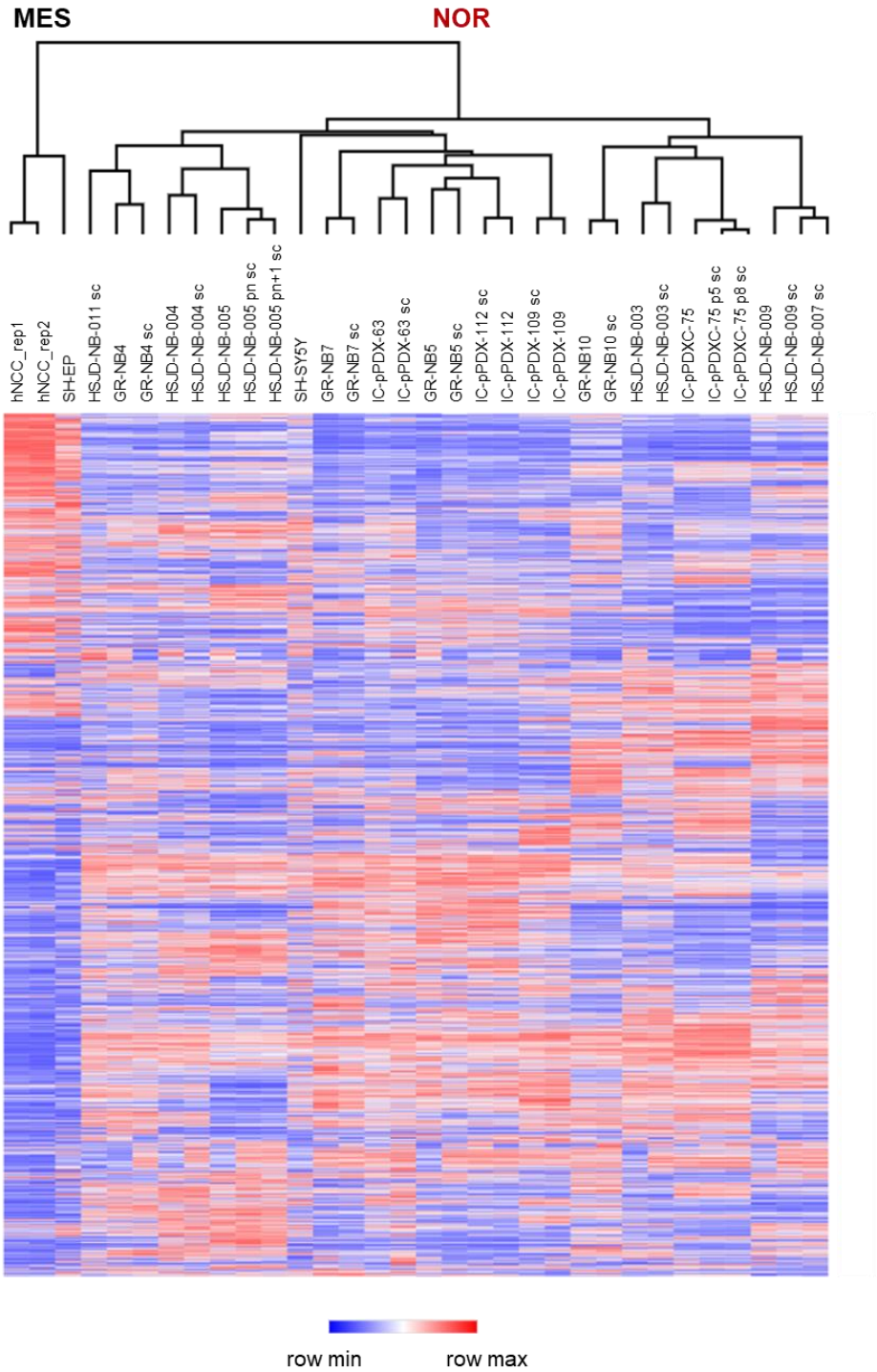

Figure S3: Detailed analyses of single-cell RNAseq of the 14 PDX models.

(**A**) The histogram highlights the contribution of the different samples to each cluster in percentage. The pie chart depicts the contribution of each sample to the total number of cells (n= 47,219). (**B**) (Top) Copy number profile inferred from WES from HSJD-NB-003 PDX model. (Bottom) InferCNV profile obtained from scRNAseq data of HSJD-NB-003. (**C**) Overview of the genomic alterations present in each

805 PDX model with the InferCNV profiles on the 14 PDX models, using 500 randomly-selected cells from
806 each sample. (**D**) Individual expression of some genes representing the mains categories identified in
807 the noradrenergic tumor cells: cell cycle, MYCN/2p-amp, sympathoblast-like and chromaffin-like. (**E**)
808 The tumor cells are colored according to their corresponding cell cycle phase (red: G1 phase; green:
809 G2/M phase; blue: S phase). (**F**) Plot of the signature of MYCN target genes[51] in the integration of all
810 PDX samples. (**G**) Unsupervised hierarchical clustering using the top 10% of genes with the highest IQR
811 (inter-quantile range) for all single cell RNAseq from PDX samples, the mesenchymal (SH-EP and
812 hNCCs) and noradrenergic (SH-SY5Y) cell lines. This shows that all PDX models clustered in the
813 noradrenergic (NOR) branch.

REFERENCES

1. Matthay, K. K. *et al.* Neuroblastoma. *Nat Rev Dis Primers* **2**, 16078 (2016).
2. Huber, K. The sympathoadrenal cell lineage: specification, diversification, and new perspectives. *Dev. Biol.* **298**, 335–343 (2006).
3. Marshall, G. M. *et al.* The prenatal origins of cancer. *Nat. Rev. Cancer* **14**, 277–289 (2014).
4. Brodeur, G. M., Seeger, R. C., Schwab, M., Varmus, H. E. & Bishop, J. M. Amplification of N-myc in untreated human neuroblastomas correlates with advanced disease stage. *Science* **224**, 1121–4 (1984).
5. Chen, Y. *et al.* Oncogenic mutations of ALK kinase in neuroblastoma. *Nature* **455**, 971–4 (2008).
6. George, R. E. *et al.* Activating mutations in ALK provide a therapeutic target in neuroblastoma. *Nature* **455**, 975–8 (2008).
7. Janoueix-Lerosey, I. *et al.* Somatic and germline activating mutations of the ALK kinase receptor in neuroblastoma. *Nature* **455**, 967–70 (2008).
8. Mosse, Y. P. *et al.* Identification of ALK as a major familial neuroblastoma predisposition gene. *Nature* **455**, 930–5 (2008).
9. Ackermann, S. *et al.* A mechanistic classification of clinical phenotypes in neuroblastoma. *Science* **362**, 1165–1170 (2018).
10. Peifer, M. *et al.* Telomerase activation by genomic rearrangements in high-risk neuroblastoma. *Nature* **526**, 700–704 (2015).
11. Valentijn, L. J. *et al.* TERT rearrangements are frequent in neuroblastoma and identify aggressive tumors. *Nat. Genet.* **47**, 1411–1414 (2015).
12. Boeva, V. *et al.* Heterogeneity of neuroblastoma cell identity defined by transcriptional circuitries. *Nat. Genet.* **49**, 1408–1413 (2017).

13. van Groningen, T. *et al.* Neuroblastoma is composed of two super-enhancer-associated differentiation states. *Nat. Genet.* **49**, 1261–1266 (2017).
14. Decaesteker, B. *et al.* TBX2 is a neuroblastoma core regulatory circuitry component enhancing MYCN/FOXM1 reactivation of DREAM targets. *Nat Commun* **9**, 4866 (2018).
15. Durbin, A. D. *et al.* Selective gene dependencies in MYCN-amplified neuroblastoma include the core transcriptional regulatory circuitry. *Nat. Genet.* **50**, 1240–1246 (2018).
16. Wang, L. *et al.* ASCL1 is a MYCN- and LMO1-dependent member of the adrenergic neuroblastoma core regulatory circuitry. *Nat Commun* **10**, 5622 (2019).
17. Rajbhandari, P. *et al.* Cross-Cohort Analysis Identifies a TEAD4-MYCN Positive Feedback Loop as the Core Regulatory Element of High-Risk Neuroblastoma. *Cancer Discov* **8**, 582–599 (2018).
18. Ross, R. A., Spengler, B. A. & Biedler, J. L. Coordinate morphological and biochemical interconversion of human neuroblastoma cells. *J. Natl. Cancer Inst.* **71**, 741–747 (1983).
19. Fernando, J. *et al.* A mesenchymal-like phenotype and expression of CD44 predict lack of apoptotic response to sorafenib in liver tumor cells. *International Journal of Cancer* **136**, E161–E172 (2015).
20. Ramos, T. L. *et al.* MSC surface markers (CD44, CD73, and CD90) can identify human MSC-derived extracellular vesicles by conventional flow cytometry. *Cell Commun. Signal* **14**, 2 (2016).
21. Saito, S. *et al.* CD44v6 expression is related to mesenchymal phenotype and poor prognosis in patients with colorectal cancer. *Oncology Reports* **29**, 1570–1578 (2013).
22. Tickle T, Tirosh I, Georgescu C, Brown M, & Haas B. inferCNV of the Trinity CTAT Project. (2019).

23. Cohen, N., Betts, D. R., Rechavi, G., Amariglio, N. & Trakhtenbrot, L. Clonal expansion and not cell interconversion is the basis for the neuroblast and nonneuronal types of the SK-N-SH neuroblastoma cell line. *Cancer Genet. Cytogenet.* **143**, 80–84 (2003).
24. Korsunsky, I. *et al.* Fast, sensitive and accurate integration of single-cell data with Harmony. *Nat. Methods* **16**, 1289–1296 (2019).
25. Chan, W. H. *et al.* RNA-seq of Isolated Chromaffin Cells Highlights the Role of Sex-Linked and Imprinted Genes in Adrenal Medulla Development. *Sci Rep* **9**, 3929 (2019).
26. Furlan, A. *et al.* Multipotent peripheral glial cells generate neuroendocrine cells of the adrenal medulla. *Science* **357**, (2017).
27. Van Limpt, V. A. E. *et al.* High delta-like 1 expression in a subset of neuroblastoma cell lines corresponds to a differentiated chromaffin cell type. *Int J Cancer* **105**, 61–69 (2003).
28. De Preter, K. *et al.* Human fetal neuroblast and neuroblastoma transcriptome analysis confirms neuroblast origin and highlights neuroblastoma candidate genes. *Genome Biol.* **7**, R84 (2006).
29. Goridis, C. & Rohrer, H. Specification of catecholaminergic and serotonergic neurons. *Nature Reviews Neuroscience* **3**, 531–541 (2002).
30. Pattyn, A., Morin, X., Cremer, H., Goridis, C. & Brunet, J. F. The homeobox gene Phox2b is essential for the development of autonomic neural crest derivatives. *Nature* **399**, 366–70 (1999).
31. Rohrer, H. Transcriptional control of differentiation and neurogenesis in autonomic ganglia. *Eur J Neurosci* **34**, 1563–73 (2011).
32. van Groningen, T. *et al.* A NOTCH feed-forward loop drives reprogramming from adrenergic to mesenchymal state in neuroblastoma. *Nat Commun* **10**, 1530 (2019).

33. Dong, R. *et al.* Single-Cell Characterization of Malignant Phenotypes and Developmental Trajectories of Adrenal Neuroblastoma. *Cancer Cell* (2020) doi:10.1016/j.ccell.2020.08.014.
34. Asgharzadeh, S. *et al.* Clinical significance of tumor-associated inflammatory cells in metastatic neuroblastoma. *J. Clin. Oncol.* **30**, 3525–3532 (2012).
35. Piskareva, O. *et al.* The development of cisplatin resistance in neuroblastoma is accompanied by epithelial to mesenchymal transition in vitro. *Cancer Lett.* **364**, 142–155 (2015).
36. Debruyne, D. N. *et al.* ALK inhibitor resistance in ALK(F1174L)-driven neuroblastoma is associated with AXL activation and induction of EMT. *Oncogene* **35**, 3681–3691 (2016).
37. Lumb, R. & Schwarz, Q. Sympathoadrenal neural crest cells: the known, unknown and forgotten? *Dev. Growth Differ.* **57**, 146–157 (2015).
38. Olsen, R. R. *et al.* MYCN induces neuroblastoma in primary neural crest cells. *Oncogene* **36**, 5075–5082 (2017).
39. Tsubota, S. & Kadomatsu, K. Origin and initiation mechanisms of neuroblastoma. *Cell Tissue Res.* **372**, 211–221 (2018).
40. Dun, S. L., Brailoiu, G. C., Yang, J., Chang, J. K. & Dun, N. J. Cocaine- and amphetamine-regulated transcript peptide and sympatho-adrenal axis. *Peptides* **27**, 1949–1955 (2006).
41. El Faitwri, T. & Huber, K. Expression pattern of delta-like 1 homolog in developing sympathetic neurons and chromaffin cells. *Gene Expr Patterns* **30**, 49–54 (2018).
42. Schütz, B., Schäfer, M. K., Eiden, L. E. & Weihe, E. Vesicular amine transporter expression and isoform selection in developing brain, peripheral nervous system and gut. *Brain Res Dev Brain Res* **106**, 181–204 (1998).

43. Weihe, E., Schäfer, M. K., Erickson, J. D. & Eiden, L. E. Localization of vesicular monoamine transporter isoforms (VMAT1 and VMAT2) to endocrine cells and neurons in rat. *J Mol Neurosci* **5**, 149–164 (1994).

44. Wildner, H., Gierl, M. S., Strehle, M., Pla, P. & Birchmeier, C. Insm1 (IA-1) is a crucial component of the transcriptional network that controls differentiation of the sympatho-adrenal lineage. *Development* **135**, 473–481 (2008).

45. Ashoor, H. *et al.* HMCan: a method for detecting chromatin modifications in cancer samples using ChIP-seq data. *Bioinformatics* **29**, 2979–2986 (2013).

46. Wolock, S. L., Lopez, R. & Klein, A. M. Scrublet: Computational Identification of Cell Doublets in Single-Cell Transcriptomic Data. *Cell Syst* **8**, 281-291.e9 (2019).

47. Butler, A., Hoffman, P., Smibert, P., Papalexi, E. & Satija, R. Integrating single-cell transcriptomic data across different conditions, technologies, and species. *Nature Biotechnology* **36**, 411–420 (2018).

48. Stuart, T. *et al.* Comprehensive Integration of Single-Cell Data. *Cell* **177**, 1888-1902.e21 (2019).

49. Franzén, O., Gan, L.-M. & Björkegren, J. L. M. PanglaoDB: a web server for exploration of mouse and human single-cell RNA sequencing data. *Database (Oxford)* **2019**, (2019).

50. Freytag, S., Tian, L., Lönnstedt, I., Ng, M. & Bahlo, M. Comparison of clustering tools in R for medium-sized 10x Genomics single-cell RNA-sequencing data. *F1000Res* **7**, 1297 (2018).

51. Valentijn, L. J. *et al.* Functional MYCN signature predicts outcome of neuroblastoma irrespective of MYCN amplification. *Proc. Natl. Acad. Sci. U.S.A.* **109**, 19190–19195 (2012).